J. Fluid Mech. (2012), *vol.* 697, *pp.* 175–203.
doi:10.1017/jfm.2012.51

Turbulence and internal waves in stably-stratified channel flow with temperature-dependent fluid properties

Francesco Zonta[1,2], Miguel Onorato[2] and Alfredo Soldati[1]†‡

[1] Centro Interdipartimentale di Fluidodinamica e Idraulica and Dipartimento di Energetica e Macchine, Università degli Studi di Udine, via delle Scienze 208, 33100 Udine, Italy

[2] Dipartimento di Fisica Generale, Università degli Studi di Torino, via Pietro Giuria 1, 10125 Torino, Italy

(Received 5 August 2011; revised 9 November 2011; accepted 22 January 2012; first published online 7 March 2012)

Direct numerical simulation (DNS) is used to study the behaviour of stably-stratified turbulent channel flow with temperature-dependent fluid properties: specifically, viscosity (μ) and thermal expansion coefficient (β). The governing equations are solved using a pseudo-spectral method for the case of turbulent water flow in a channel. A systematic campaign of simulations is performed in the shear Richardson number parameter space ($Ri_\tau = Gr/Re_\tau$, where Gr is the Grashof number and Re_τ the shear Reynolds number), imposing constant-temperature boundary conditions. Variations of Ri_τ are obtained by changing Re_τ and keeping Gr constant. Independently of the value of Ri_τ, all cases exhibit an initial transition from turbulent to laminar flow. A return transition to turbulence is observed only if Ri_τ is below a threshold value (which depends also on the flow Reynolds number). After the transient evolution of the flow, a statistically-stationary condition occurs, in which active turbulence and internal gravity waves (IGW) coexist. In this condition, the transport efficiency of momentum and heat is reduced considerably compared to the condition of non-stratified turbulence. The crucial role of temperature-dependent viscosity and thermal expansion coefficient is directly demonstrated. The most striking feature produced by the temperature dependence of viscosity is flow relaminarization in the cold side of the channel (where viscosity is higher). The opposite behaviour, with flow relaminarization occurring in the hot side of the channel, is observed when a temperature-dependent thermal expansion coefficient is considered. We observe qualitative and quantitative modifications of structure and wall-normal position of internal waves compared to previous results obtained for uniform or quasi-uniform fluid properties. From the trend we observe in the investigated low-Reynolds-number range, we can hypothesize that, whereas the effects of temperature-dependent viscosity may be masked at higher Reynolds number, the effects of temperature-dependent thermal expansion coefficient will persist.

Key words: internal waves, stratified turbulence, wave–turbulence interactions

† Email address for correspondence: soldati@uniud.it

‡ Present address: Department of Fluid Mechanics, CISM, 33100, Udine, Italy.

1. Introduction

Turbulence subject to thermal stratification (stratified flow) is of great interest due to the importance in geophysical, industrial and environmental applications. In the atmosphere, stable stratification of air is induced by thermal inversion. In urban areas, stratification is detrimental for air quality, since pollutants released by road traffic and factories remain trapped in the stably-stratified layer of air. In terrestrial water bodies (oceans, lakes or rivers) stratified turbulence influences the vertical transport of nutrients and chemical/biological species (van deer Lee & Umlauf 2011). In industrial applications, stratification may strongly reduce mixing and in turn heat transfer.

Stable stratification often occurs in the presence of large temperature gradients. The analysis of stably-stratified turbulent flows is usually performed assuming constant and uniform thermophysical fluid properties. However, most fluids exhibit temperature-dependent thermophysical properties with significant variations for large temperature differences. Viscosity of water decreases from $\mu \simeq 0.8 \times 10^{-3}$ Pa s at 303 K to $\mu \simeq 0.4 \times 10^{-3}$ Pa s at 343 K (a value half the size), while the thermal expansion coefficient increases from $\beta \simeq 3 \times 10^{-4}$ K^{-1} at 303 K to $\beta \simeq 5.7 \times 10^{-4}$ K^{-1} at 343 K (a value almost twice the size). Ignoring these variations may produce inaccurate prediction of momentum and heat transfer rates.

Despite the number of experiments and atmospheric observations of stratified turbulence (see Turner 1973; Fernando 1991; Fritts & Alexander 2003), the phenomenology and evolution of the flow are not yet fully understood. Experimental works were performed by Arya (1975) and Komori *et al.* (1983), among others. Arya (1975) considered a stratified boundary layer of air developing over a cooled/heated wall and observed that stable stratification reduces the skin friction coefficient, the Nusselt number and turbulence intensities. No flow relaminarization was observed. Similar conclusions were given by Komori *et al.* (1983) who analysed the stratified flow obtained by condensing steam over the upper surface of an open channel. Under strong stratification, Komori *et al.* (1983) also observed wave-like motions and counter-gradient momentum and heat flux.

The effect of thermal stratification on homogeneous turbulence was investigated using direct numerical simulation (DNS) by Gerz & Yamazaki (1993) and by Metais & Herring (1989) (among others). There are relatively few results produced by numerical simulations of the fully developed wall turbulence under stable density stratification. Stably-stratified turbulent channel flow was investigated by Garg *et al.* (2000) using large-eddy simulation (LES) of incompressible flow for different stratification levels. Rather than solving the energy equation for temperature distribution, they solved a scalar transport equation for density. Equations written in variable viscosity and diffusivity form (to allow for quasi-uniform properties) were solved by a hybrid spectral finite-difference discretization and a fractional step algorithm. Simulations considered a turbulent channel flow of air at shear Reynolds number $Re_\tau = 180$ and Prandtl number $Pr = 0.71$. The friction Richardson number was defined as $Ri_\tau = \Delta\rho g h/(\rho_0 u_\tau^2)$, where $\Delta\rho$ is the density difference across the channel, g is the acceleration due to gravity, h is the channel half-height, ρ_0 is a reference density and u_τ is the friction velocity. Three different stratification regimes were identified, depending on the shear Richardson number: a *buoyancy-affected* regime ($Ri_\tau < 30$), in which turbulence is partially suppressed; a *buoyancy-controlled* regime ($30 < Ri_\tau < 45$) with a temporary flow relaminarization in one half of the channel followed by a sharp transition that restores a symmetric turbulent flow; a *buoyancy-dominated* regime ($Ri_\tau > 45$), characterized by a rapid relaminarization of the whole flow. The shear Richardson number Ri_τ was found to be better than the gradient

Richardson number $Ri_g = N^2/S^2$ (N being the buoyancy frequency and S the mean shear rate) for the characterization of the flow regimes in wall-bounded flows.

In a similar study, Armenio & Sarkar (2002) used LES to simulate an incompressible flow under the Boussinesq approximation and solved for a scalar density transport equation. Maintaining all thermophysical fluid properties constant, they examined a closed channel flow at $Re_\tau = 180$, $Pr = 0.71$ with different shear Richardson numbers (up to $Ri_\tau = 480$). In contrast to the results of Garg *et al.* (2000), Armenio & Sarkar (2002) did not observe flow relaminarization. They did observe that increasing the Richardson number decreased the near-wall turbulence activity. They argued that the relaminarization phenomenon observed by Garg *et al.* (2000) was just a transient, since in their simulations it was always followed by a sharp transition back to turbulence. They finally verified that the results of Garg *et al.* (2000) were not consistent with the linear stability analysis of plane Poiseuille stratified flows (at $Pr = 1$) of Gage & Reid (1968).

DNS of stably-stratified turbulence in a closed channel was performed by Iida, Kasagi & Nagano (2002) using the Boussinesq approximation and constant thermophysical properties, and solving the energy equation for temperature distribution. They showed that, at high Richardson number, velocity fluctuations may lose symmetry about the channel centreline. More recently, Lessani & Zainali (2009) used LES to study a stably-stratified channel flow under non-Boussinesq conditions. They used a low-Mach-number approximation for fluid density variation and showed that, at $Re_\tau = 180$, $Pr = 0.71$ and $Ri_\tau \leqslant 60$, for strong temperature gradient, the velocity field may be asymmetric. Unlike in Iida *et al.* (2002) (where thermophysical properties of the fluid were uniform), the flow asymmetry in Lessani & Zainali (2009) was purely induced by non-uniform thermophysical properties.

In view of the literature survey given above, the aim of this work is to contribute to the current physical understanding by performing accurate numerical experiments in a stably-stratified channel flow of water in which fluid viscosity (μ) and fluid thermal expansion coefficient (β) vary with temperature. Simulations were based on a full pseudo-spectral method for the numerical solution of the momentum and energy equations. The numerical methodology, already applied in Zonta, Marchioli & Soldati (2012) is described in § 2. Simulations (DNS) are performed at reference Reynolds, Prandtl and Richardson numbers using a variable-properties formulation of the Navier–Stokes equations.

Starting from a neutrally-buoyant channel flow with temperature as a passive scalar, we turn on the gravitational field and we follow the time evolution of the flow under stable stratification. One-sided turbulence may be sustained either by an inhomogeneous distribution of viscosity or by an inhomogeneous distribution of thermal expansion coefficient. With temperature-dependent viscosity, active turbulence is observed only in the upper part of the channel (hotter fluid) with flow laminarization occurring in the lower part (colder fluid). The situation reverses with temperature-dependent thermal expansion coefficient (turbulence is sustained only in the lower, and colder, part of the channel). Only for a specific value of parameters ($Re_\tau = 150$ or $Ri_\tau = 498$) are the effects of temperature-dependent viscosity of the same order as the effects of temperature-dependent thermal expansion coefficient. In this case the two effects have similar importance. At lower Reynolds numbers ($Re_\tau = 110$ in this work) effects of temperature-dependent viscosity are more important than those of temperature-dependent thermal expansion coefficient. The opposite occurs at higher Reynolds numbers ($Re_\tau = 180$ in this work): effects of temperature-dependent thermal expansion coefficient are larger than effects of temperature-dependent viscosity

(which seem to be masked by predominant inertial effects). These trends lead us to hypothesize that at higher Reynolds number only the effects of temperature-dependent thermal expansion coefficient will be important.

2. Governing equations

We consider an incompressible and Newtonian turbulent flow of water in a plane channel with differentially-heated walls. The reference geometry consists of two horizontal (infinite) flat parallel walls; the origin of the coordinate system is located at the centre of the channel and the x-, y- and z-axes point in the streamwise, spanwise and wall-normal directions. Indicating by h^* the half-channel height, the size of the channel is $4\pi h^* \times 2\pi h^* \times 2h^*$ in x, y and z, respectively. The bottom wall is kept at a uniform low temperature ($T^*_{bottom} = T^*_C$), whereas the top wall is kept at a uniform high temperature ($T^*_{top} = T^*_H$). As a consequence, there is a constant negative temperature difference $\Delta T^* = (T^*_{bottom} - T^*_{top})$ between the bottom and the top walls which causes a stable buoyancy effect (the gravitational acceleration acting downward along the wall-normal direction). In dimensional form (denoted by the superscript *) and using the Einstein notation (repeated index implies summation), conservation of mass, momentum and energy of the fluid is described by the following set of three-dimensional time-dependent equations:

$$\frac{\partial u_i^*}{\partial x_i^*} = 0, \tag{2.1}$$

$$\rho^* \frac{\partial u_i^*}{\partial t^*} + \rho^* u_j^* \frac{\partial u_i^*}{\partial x_j^*} = \frac{\partial}{\partial x_j^*}\left(\mu^* \frac{\partial u_i^*}{\partial x_j^*}\right) - \frac{\partial p^*}{\partial x_i^*} + \left(\rho^* - \rho^*_{ref}\right) g_i^* + \delta^*_{1,i}, \tag{2.2}$$

$$\rho^* c_p^* \frac{\partial T^*}{\partial t^*} + \rho^* c_p^* u_j^* \frac{\partial T^*}{\partial x_j^*} = \frac{\partial}{\partial x_j^*}\left(\lambda^* \frac{\partial^2 T^*}{\partial x_j^{*2}}\right), \tag{2.3}$$

where u_i^* is the ith component of the velocity vector, g_i^* is the ith component of the gravitational acceleration vector, p^* is the fluctuating kinematic pressure, $\delta^*_{1,i}$ is the mean pressure gradient that drives the flow, T^* is temperature, ρ^* is density, μ^* is viscosity, λ^* is thermal conductivity and c_p^* is specific heat. Variables in (2.1)–(2.3) are made dimensionless as follows:

$$\rho = \frac{\rho^*}{\rho^*_{ref}}, \quad \mu = \frac{\mu^*}{\mu^*_{ref}}, \quad \lambda = \frac{\lambda^*}{\lambda^*_{ref}}, \quad c_p = \frac{c_p^*}{c^*_{p,ref}}, \tag{2.4}$$

$$\boldsymbol{x} = \frac{\boldsymbol{x}^*}{h^*}, \quad \boldsymbol{u} = \frac{\boldsymbol{u}^*}{u^*_\tau}, \quad t = \frac{t^* u^*_\tau}{h^*}, \quad p = \frac{p^*}{\rho^*_{ref} u^{*2}_\tau}, \quad T = \frac{T^* - T^*_{ref}}{\Delta T^*/2}. \tag{2.5}$$

Subscript *ref* is used to represent thermophysical fluid properties at the reference temperature, $T^*_{ref} = (T^*_H + T^*_C)/2$. The reference velocity for non-dimensionalization is the shear (or friction) velocity $u^*_{ref} = u^*_\tau$. We compute u^*_τ directly from the reference Reynolds number, defined as $Re_\tau = \rho^*_{ref} u^*_\tau h^*/\mu^*_{ref}$ (Zonta *et al.* 2012). According to this approach, Re_τ is a 'macroscopic' input parameter of the numerical scheme. Two other dimensionless numbers, the reference Prandtl number, $Pr = (\mu^*_{ref} c^*_{p,ref})/\lambda^*_{ref}$, and the reference Grashof number, $Gr = (g^* \beta^*_{ref} \Delta T^* (2h^*)^3)/(\nu^*_{ref})^2$, are used as input parameters of the numerical scheme. In the definition of the Grashof number, $\beta^*_{ref} = -(1/\rho^*)(\partial \rho^*/\partial T^*)_p$ and $\nu^*_{ref} = \mu^*_{ref}/\rho^*_{ref}$ are the thermal expansion coefficient and the kinematic viscosity at the reference temperature. The key parameter for stratified flows is the Richardson number Ri (i.e. the ratio between buoyancy and

inertia). Throughout this study, the shear Richardson number $Ri_\tau = Gr/Re_\tau^2$ is adopted. Garg *et al.* (2000) have shown that this parameter is suitable for the characterization of the flow regimes in wall-bounded stratified flows.

In this study, all the thermophysical properties of the fluid, with the exception of dynamic viscosity μ^* and thermal expansion coefficient β^*, are kept uniform. To put this in context, let us consider a physical temperature difference of 40 K between the walls ($T_C^* = 303$ K and $T_H^* = 343$ K), which corresponds to the temperature difference taken in our simulations. The variation of the dynamic viscosity and of the thermal expansion coefficient of water (with respect to their reference value) is $\Delta\mu\,(\%) = (|\mu^*_{343\ \mathrm{K}} - \mu^*_{303\ \mathrm{K}}|)/\mu^*_{ref} \simeq 0.73$ and $\Delta\beta\,(\%) = (|\beta^*_{343\ \mathrm{K}} - \beta^*_{303\ \mathrm{K}}|)/\beta^*_{ref} \simeq 0.59$, respectively. Variations of ρ, λ and c_p are at least an order of magnitude lower (Incropera & Dewitt 1985), confirming that the assumption $\rho = \lambda = c_p = 1$ is valid. Within the framework of the present paper, dissipative heating is neglected and volumetric changes due to thermal diffusion are not important. Throughout the paper, results for stably-stratified flows with uniform and non-uniform thermophysical properties of the fluid are shown. The dimensionless governing balance equations for each specific case are discretized using a pseudo-spectral method based on transforming the field variables into wavenumber space, through Fourier representations for the periodic (homogeneous) directions x and y, and Chebychev representation for the wall-normal (non-homogeneous) direction z. Note that periodicity in x and y is assumed for both velocity and temperature.

As commonly done in pseudospectral methods, the convective nonlinear terms are first computed in the physical space and then transformed to the wavenumber space using a de-aliasing procedure based on the 2/3-rule; derivatives are evaluated directly in the wavenumber space to maintain spectral accuracy. Further details can be found in Zonta *et al.* (2012) and Soldati & Banerjee (1998).

3. Summary of the simulations

The fluid is driven by an imposed pressure gradient and flows between the two walls, which are kept at constant temperature T_H^* and T_C^*, whereas buoyancy acts along the wall-normal direction (z). An extensive campaign of simulations is performed (table 1). The spatial resolution of each simulation is chosen to fulfil the requirements imposed by the DNS. In the present configuration, the stable temperature profile reduces the vorticity fluctuations, and thus the rate of kinetic energy dissipation. Therefore, although stratification will cause a decrease of some of the (largest) length scales, the Kolmogorov scale is larger in stratified cases than in neutral ones (Coleman, Ferziger & Spalart 1992); a grid adequate for a neutrally-buoyant flow ($128 \times 128 \times 257$), also resolves the stratified turbulent velocity field. In this work we decided to run the numerical simulation using up to $256 \times 256 \times 257$ grid points (see table 1). Simulations labelled 'Boussinesq' are the base simulations with uniform thermophysical properties. In simulations labelled '$\mu(T)$' viscosity is a function of temperature. Exponential (or Arrhenius type) relations are usually employed to represent temperature-dependent viscosity. Here we adopted the following relation (Popiel & Wojtkowiak 1998; Zonta *et al.* 2012):

$$\mu^*(T^*) = A \times 10^{B/(T^* - C)} \tag{3.1}$$

where T^* is the local fluid temperature in K, while A, B and C are constants associated with the specific fluid considered. For water, $A = 2.414 \times 10^{-5}$, $B = 247.8$ and $C = 140$. A graphical representation of (3.1) is given in figure 1(*a*).

Simulations	Re_τ	Ri_τ	$Ri'_\tau \left(=\frac{Ri_\tau}{16}\right)$	Grid	Thermophysical properties	
$T110-$Boussinesq	110	926	58	$256\times256\times257$	Uniform	Transient
$T150-$Boussinesq	150	498	31	$256\times256\times257$	Uniform	
$T180-$Boussinesq	180	346	22	$256\times256\times257$	Uniform	
$SS110-$Boussinesq	110	926	58	$128\times128\times257$	Uniform	Steady state
$SS110-\mu(T)$	110	926	58	$128\times128\times257$	$\mu=\mu(T)$ (3.1)	
$SS110-\beta(T)$	110	926	58	$128\times128\times257$	$\beta=\beta(T)$ (3.2)	
$SS150-$Boussinesq	150	498	31	$128\times128\times257$	Uniform	
$SS150-\mu(T)$	150	498	31	$128\times128\times257$	$\mu=\mu(T)$ (3.1)	
$SS150-\beta(T)$	150	498	31	$128\times128\times257$	$\beta=\beta(T)$ (3.2)	
$SS180-$Boussinesq	180	346	22	$128\times128\times257$	Uniform	
$SS180-\mu(T)$	180	346	22	$128\times128\times257$	$\mu=\mu(T)$ (3.1)	
$SS180-\beta(T)$	180	346	22	$128\times128\times257$	$\beta=\beta(T)$ (3.2)	
$NB110$	110	0	0	$128\times128\times129$	Uniform	Neutrally buoyant
$NB150$	150	0	0	$256\times256\times257$	Uniform	
$NB180$	180	0	0	$256\times256\times257$	Uniform	

TABLE 1. Stably-stratified turbulent channel flow: summary of the simulations parameters.

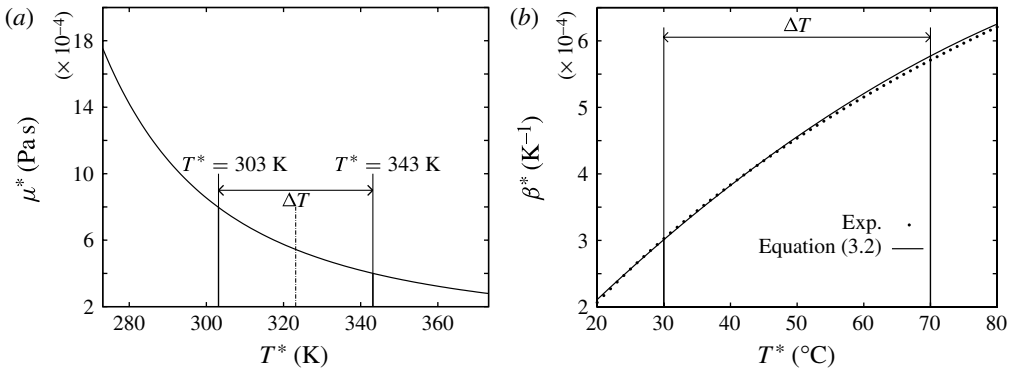

FIGURE 1. (*a*) Viscosity (μ^*) of water as a function of temperature for 273 K $< T^* <$ 373 K. The temperature difference (ΔT) between the hot wall and the cold wall considered in our simulations is also shown. (*b*) Thermal expansion coefficient (β^*) of water as a function of temperature for 20 °C $< T^* <$ 80 °C. Experimental data (symbols, Incropera & Dewitt 1985) and interpolation curve (line, (3.2)) are shown.

In simulations labelled '$\beta(T)$' the thermal expansion coefficient changes with temperature. Experimental values of $\beta^*(T)$ (Incropera & Dewitt 1985) are shown in figure 1(*b*). A fitting equation (figure 1*b*) of the experimental data is given by

$$\beta^*(T) = \beta^*_{ref}\left(1 + 0.29 \times T - 0.037 \times T^2\right), \tag{3.2}$$

where T is the dimensionless temperature (see § 2).

A temperature difference $\Delta T^* = T^*_H - T^*_C = 40$ K is imposed between the hot and the cold wall, which are kept at $T_H = 343$ K and $T_C = 303$ K, respectively. All simulations are performed at reference Prandtl number $Pr = 3$ and Grashof number $Gr = 1.12 \times 10^7$. DNS of stratified turbulence at $Pr > 1$ (water) is one of the contributions of this work to the archival literature, since most stratified turbulence has been analysed at $Pr = 1$ or $Pr = 0.71$ (air). Three different reference shear Reynolds number are considered in this study: $Re_\tau = 110$, $Re_\tau = 150$ and $Re_\tau = 180$. As a consequence, computations are run at three different values of the shear Richardson number, $Ri_\tau = Gr/Re_\tau^2$: $Ri_\tau = 926$ ($Re_\tau = 110$), $Ri_\tau = 498$ ($Re_\tau = 150$) and $Ri_\tau = 346$ ($Re_\tau = 180$). Comparison of our results with those of Garg *et al.* (2000) is possible if we consider a modified Richardson number, $Ri'_\tau = Ri_\tau/16$, as the key parameter. Using this definition, we obtain $Ri'_\tau = 58$, $Ri'_\tau = 31$ and $Ri'_\tau = 22$. A comprehensive overview of the simulations parameters is provided in table 1.

4. Results and discussion

Results of the simulations will be presented by following the dynamical evolution of a stably-stratified channel flow from the initial transient, up to the statistical steady state. The initial transient is a two-stage process. In the first stage, flow laminarization is always observed, regardless of the Richardson number. In the second stage, the flow can either remain laminar or become turbulent, depending on the value of the Richardson number (in our simulations, we have observed both of these evolutions). After this initial transient, the flow reaches a new steady-state condition. Flow field statistics will be analysed and discussed carefully, and the role of temperature-

dependent fluid properties will be pointed out. Statistical results will be also linked in a phenomenological causal relationship to coherent flow structures (internal waves).

4.1. *Transient evolution of the flow*

In this section, we consider the transient evolution of a stably-stratified turbulent channel flow. We started our simulations from a realization of equilibrium channel flow with temperature considered a passive scalar (neutrally buoyant simulations at $Re_\tau = 110, 150, 180$ in table 1). Then, the development of the flow under stable stratification at three different values of the Richardson number ($Ri_\tau = 346$, $Ri_\tau = 498$ and $Ri_\tau = 926$) and for uniform thermophysical properties is investigated.

The time evolution of the flow, analysed in figure 2, reveals a two-stage process. During the first stage of the process (up to $t \simeq 16$, figure 2), flow laminarization is observed for each value of the Richardson number. The turbulent kinetic energy, $E_k = (1/2)\overline{u_i^2}$, is completely suppressed (inset of figure 2*a*), whereas the Nusselt number $Nu_c = (\partial\overline{T}/\partial z)|_w$, which quantifies the heat transfer rate at the wall (subscript w), drops rapidly by more than a factor of 5 (inset of figure 2*b*). Overbars indicate a space average over the entire volume (for E_k), or a space average over the wall surfaces (for Nu_c). Interestingly (insets of figure 2*a,b*), decay is nearly monotonic for Nu_c but oscillatory for E_k (Garg *et al.* 2000; Metais & Herring 1989; Lienhard V & Van Atta 1990).

During the second stage of the process (for $t > 16$, figure 2) the flow behaves differently, depending on the value of the Richardson number: the flow remains laminar for $Ri_\tau = 926$ (solid line, $Re_\tau = 110$), whereas a return transition to turbulence occurs for $Ri_\tau = 498$ (dashed line, $Re_\tau = 150$) and $Ri_\tau = 346$ (dotted line, $Re_\tau = 180$). Our results agree partially with the linear theory of Gage & Reid (1968), which prescribes an explicit relation between the critical Richardson number for stability and the Reynolds number of the flow. Gage & Reid (1968) considered a stably-stratified channel flow with imposed temperature at the walls, equivalent to the problem considered in the present paper. They used the centreline Reynolds number (Re_c) and the centreline Richardson number (Ri_c) as dimensionless parameters. The centreline Reynolds number Re_c can be computed from the shear Reynolds number as $Re_c = Re_\tau^2/2$ (Armenio & Sarkar 2002). The corresponding critical shear Richardson number ($Ri_{\tau,cr}$) is $Ri_{\tau,cr} = 2Ri_c Re_\tau^2$, with Ri_c the critical Richardson number given by Gage & Reid (1968). For the cases considered in our simulations, $Ri_c \simeq 4.9 \times 10^{-5}$ for $Re_\tau = 110$, $Ri_c \simeq 8.2 \times 10^{-3}$ for $Re_\tau = 150$ and $Ri_c \simeq 1.36 \times 10^{-2}$ for $Re_\tau = 180$. As a consequence, laminar Poiseuille flow is linearly stable if (i) $Ri_\tau > 1.2$ for $Re_\tau = 110$, (ii) $Ri_\tau > 370$ for $Re_\tau = 150$ and (iii) $Ri_\tau > 881$ for $Re_\tau = 180$. These results are consistent with the observations made in figure 2 that the flow remains laminar for $Ri_\tau = 926$ ($Re_\tau = 110$), whereas it undergoes a return transition to turbulence for $Ri_\tau = 498$ ($Re_\tau = 150$) and $Ri_\tau = 346$ ($Re_\tau = 180$).

To conclude, our results agree with the linear theory for $Ri_\tau = 926$ ($Re_\tau = 110$) and $Ri_\tau = 346$ ($Re_\tau = 180$); they do not agree for $Ri_\tau = 498$ ($Re_\tau = 150$). A similar deviation was noted by Armenio & Sarkar (2002) who reported on a turbulent asymptotic state at a Richardson number $Ri_\tau = 960$ (and $Re_\tau = 180$), a value larger than the critical value based on linear instability theory ($Ri_{\tau,cr} = 881$). Similarly, we observe a turbulent asymptotic state at $Ri_\tau = 498$ (and $Re_\tau = 150$), although the corresponding critical Richardson number would be $Ri_{\tau,cr} = 370$. These deviations may

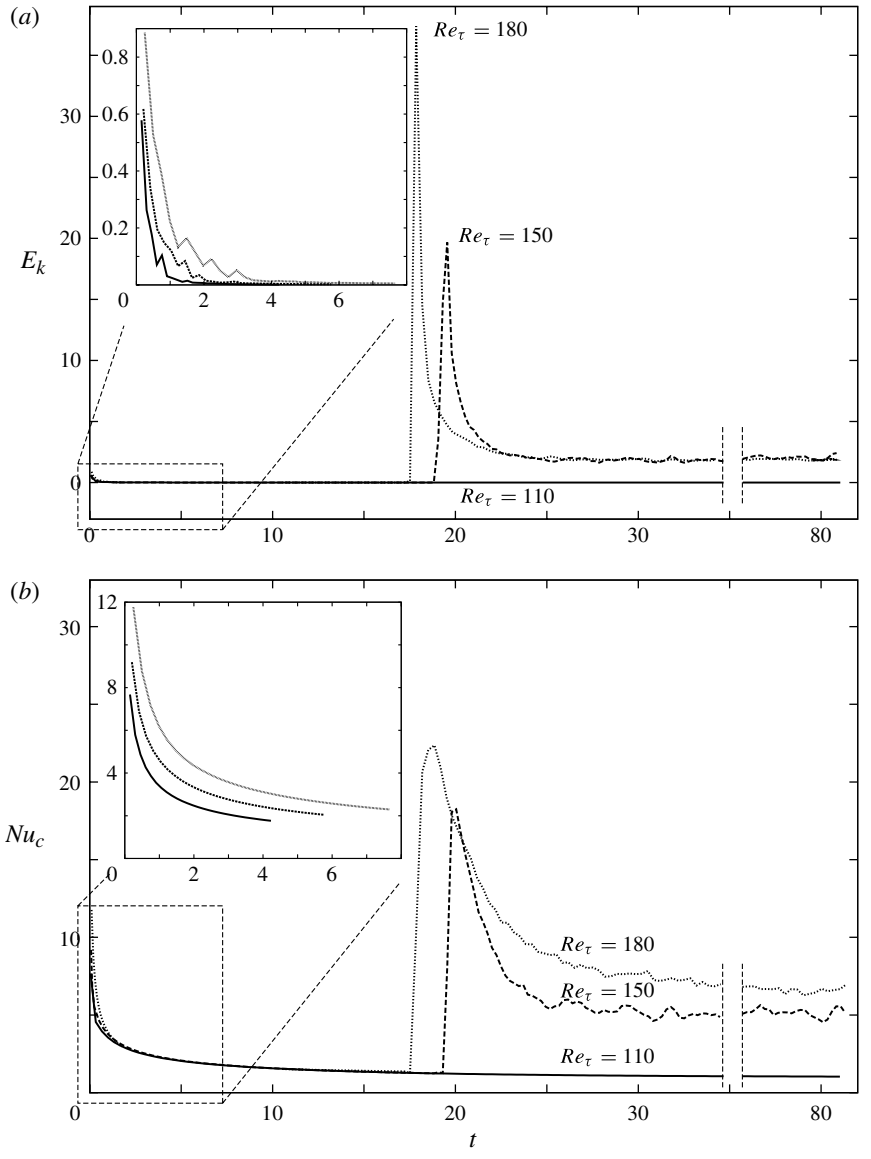

FIGURE 2. Time evolution of (*a*) turbulent kinetic energy E_k and (*b*) centreline Nusselt number Nu_c, for $Ri_\tau = 346$ ($Re_\tau = 180$, dotted line), $Ri_\tau = 498$ ($Re_\tau = 150$, dashed line) and $Ri_\tau = 926$ ($Re_\tau = 110$, solid line). Computed quantities are averaged in space over the whole domain (E_k) or over the wall surfaces (Nu_c).

indicate the existence of subcritical transition, meaning that in such situations small but finite perturbations may lead to instability even well beyond the critical Richardson number (Armenio & Sarkar 2002). Differences between our results and those of Gage & Reid (1968) may also be ascribed to the value of the Prandtl number: $Pr = 1$ in Gage & Reid (1968) and $Pr = 3$ in the present study.

A qualitative analysis of the time history of the flow is provided in figure 3 (for $Ri_\tau = 498$ and uniform thermophysical properties). Time snapshots of temperature contours on an x–z plane reveal that fully turbulent flow (figure 3*a*) is gradually

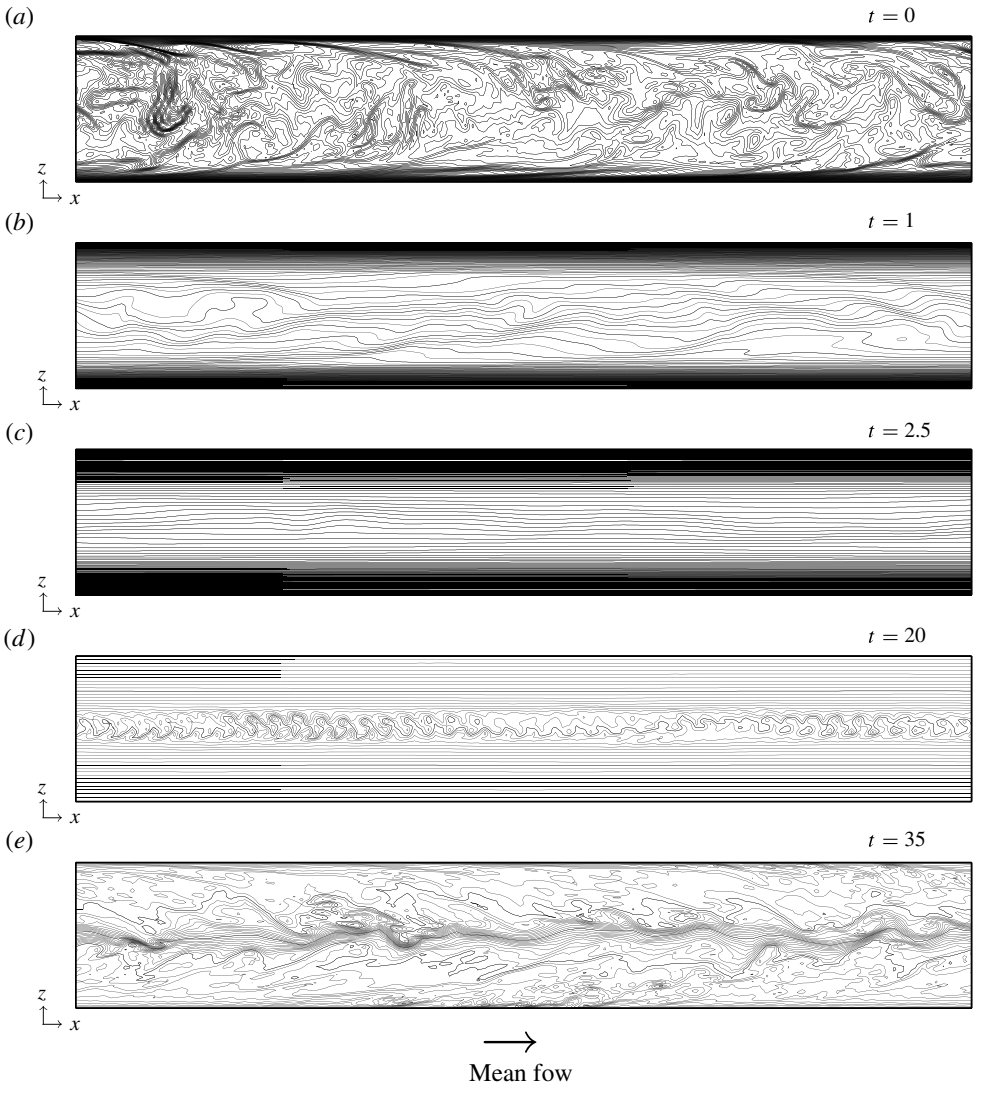

FIGURE 3. Time evolution of turbulence structures (visualized using temperature contours on an x–z plane) for the simulation at $Ri_\tau = 498$ and uniform thermophysical properties.

suppressed and the flow reaches a pseudolaminar condition (figure 3*c*). which is unstable to small disturbances, as prescribed by the linear theory (Gage & Reid 1968; Biau & Bottaro 2004). Flow instabilities arise and rolled-up vortical structures develop along the centreline of the channel (figure 3*d*). After a half-rotation of a vortical structure, cold fluid is brought above hot fluid and vice versa, inducing the formation of unstably-stratified regions of fluid. Instabilities grow and the flow reaches a new turbulent steady-state condition with overall transport rates which are smaller than the initial values of neutrally-buoyant turbulent channel flow. Elongated wavy structures are observed in the core region of the channel. These structures are called internal gravity waves (IGW) and are considered key features in stably-stratified turbulence. Internal waves will be analysed in § 4.3.

4.2. *Buoyancy effects on the steady state*

In the previous section we have observed that temporary relaminarization may occur during the transient development of an initially-turbulent stably-stratified channel flow, but a turbulent regime with a statistically steady state may be eventually reached, depending on the value of the shear Richardson number (strength of stratification). In this section we discuss how stable stratification affects flow and mixing characteristics of this new regime. The effect of the temperature-dependent viscosity and thermal expansion coefficient is also considered and discussed. This is the main contribution of this work to the archival literature. To the best of our knowledge, DNS of stably-stratified channel turbulence for $Pr > 1$ has been performed only within the assumption of constant fluid properties. In the present work, we use DNS to analyse stably-stratified channel turbulence for $Pr > 1$ and assuming temperature-dependent fluid properties (specifically, viscosity and thermal expansion coefficient). Flow statistics are obtained by time-averaging results (over a sufficiently long time window) after the statistically steady state is reached. In the following sections, to keep discussion contained, we will examine only the results relating to the simulation at $Ri_\tau = 498$ ($Re_\tau = 150$) since all the effects we wish to emphasize are evident at this Richardson number. Statistics of fluid velocities and temperature for $Ri_\tau = 346$ ($Re_\tau = 180$) and $Ri_\tau = 926$ ($Re_\tau = 110$) can be found in the Appendix.

4.2.1. *Fluid velocity statistics*

In figure 4 the mean streamwise velocity profiles, $\langle u_x \rangle$, are shown as a function of the dimensionless wall-normal coordinate $z = z^*/h^*$. Brackets indicate the average in time and in space (over the homogeneous directions). Results from simulations with uniform thermophysical properties (solid line), with temperature-dependent viscosity (dotted line) and with temperature-dependent thermal expansion coefficient (dash-dotted line) are compared. The profile of mean streamwise velocity from the simulation of neutrally-buoyant turbulent channel flow (symbols) is also included for comparison purposes.

Stable stratification suppresses wall-normal momentum transport compared to the neutrally buoyant case, where temperature is a passive scalar. Suppression of wall-normal momentum transport is the consequence of the conversion of kinetic energy into potential energy occurring when a fluid particle is displaced in the wall-normal direction within the flow field. Since the driving pressure gradient is held constant among simulations, the viscous wall stress and, therefore, the slope of the mean velocity profile in the case of stable stratification should be invariant compared to those of the neutrally-buoyant case. This is true only for stable stratification with uniform fluid properties (Lessani & Zainali 2009). The centreline velocity increases compared to the neutrally-buoyant simulation and so does the mass flow rate. The increased mass flow rate is associated with a decrease of both friction factor and Nusselt number of the flow (the driving pressure gradient being constant in all the simulations). For the Richardson number considered in this discussion ($Ri_\tau = 498$), both viscosity and thermal expansion coefficient have a dramatic impact on the behaviour of the flow field. Temperature-dependent viscosity alters the symmetry of the velocity profile, since the rate of change of $\langle u_x \rangle$ with z (velocity gradient at the wall) is directly linked to the local value of viscosity. In particular, velocity gradients are higher at the hot wall (lower viscosity) and lower at the cold wall (higher viscosity). The symmetry of the velocity profile is lost even in the case of temperature-dependent thermal expansion coefficient. A physical explanation of this

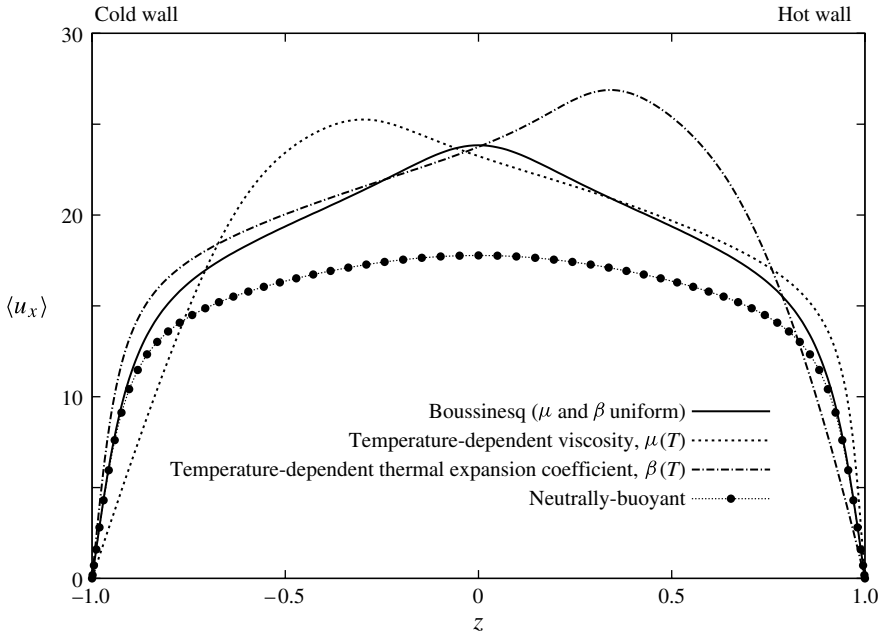

FIGURE 4. Mean fluid streamwise velocity $\langle u_x \rangle$ for stably-stratified turbulent channel flow at $Ri_\tau = 498$ ($Re_\tau = 150$): comparison between simulations with uniform thermophysical properties (solid line) and simulations with temperature-dependent viscosity (dashed line) and temperature-dependent thermal expansion coefficient (dash-dotted line). Results from simulation of neutrally-buoyant turbulent channel flow (symbols) are also included.

result (together with implications for turbulence modulation) will be given within the discussion on turbulence fluctuations.

The root mean square (r.m.s.) of the fluid velocity fluctuations in each direction is shown in figure 5. A first comparison is made between stable stratification with uniform thermophysical properties (solid line) and neutrally-buoyant turbulent flow (symbols). This comparison is useful to single out those effects induced purely by stratification. In the near-wall region, $|z - z_w| < 0.3$ (z_w being the position of the wall), none of the velocity fluctuation profiles is significantly changed, so that typical near-wall turbulence is maintained. In the buffer region, up to $|z - z_w| \simeq 0.6$, $\langle (u'_x)_{rms} \rangle$ and $\langle (u'_y)_{rms} \rangle$ increase, whereas $\langle (u'_z)_{rms} \rangle$ decreases. The increase of streamwise and spanwise fluctuations is caused by a higher velocity gradient which enhances turbulent production in this region (Iida *et al.* 2002). In the core region of the channel, $|z| < 0.4$, $\langle (u'_x)_{rms} \rangle$ and $\langle (u'_y)_{rms} \rangle$ decrease markedly, whereas $\langle (u'_z)_{rms} \rangle$ takes a local maximum which is not observed in the neutrally-buoyant flow. The characteristic shape of $\langle (u'_z)_{rms} \rangle$ is associated with internal waves (see § 4.3 for details). The observations made above indicate that the structural characteristics of turbulence are not affected by stratification in the near-wall region ($|z - z_w| < 0.3$), since the ratio between the wall-normal and the streamwise fluctuations, $\langle (u'_z)_{rms} \rangle / \langle (u'_x)_{rms} \rangle$ (not shown for brevity) is nearly unchanged. However, a strong decrease of $\langle (u'_z)_{rms} \rangle / \langle (u'_x)_{rms} \rangle$ occurs in the buffer region, demonstrating that in this region stratification damps the transfer of energy from streamwise to wall-normal velocity fluctuations (Armenio & Sarkar 2002).

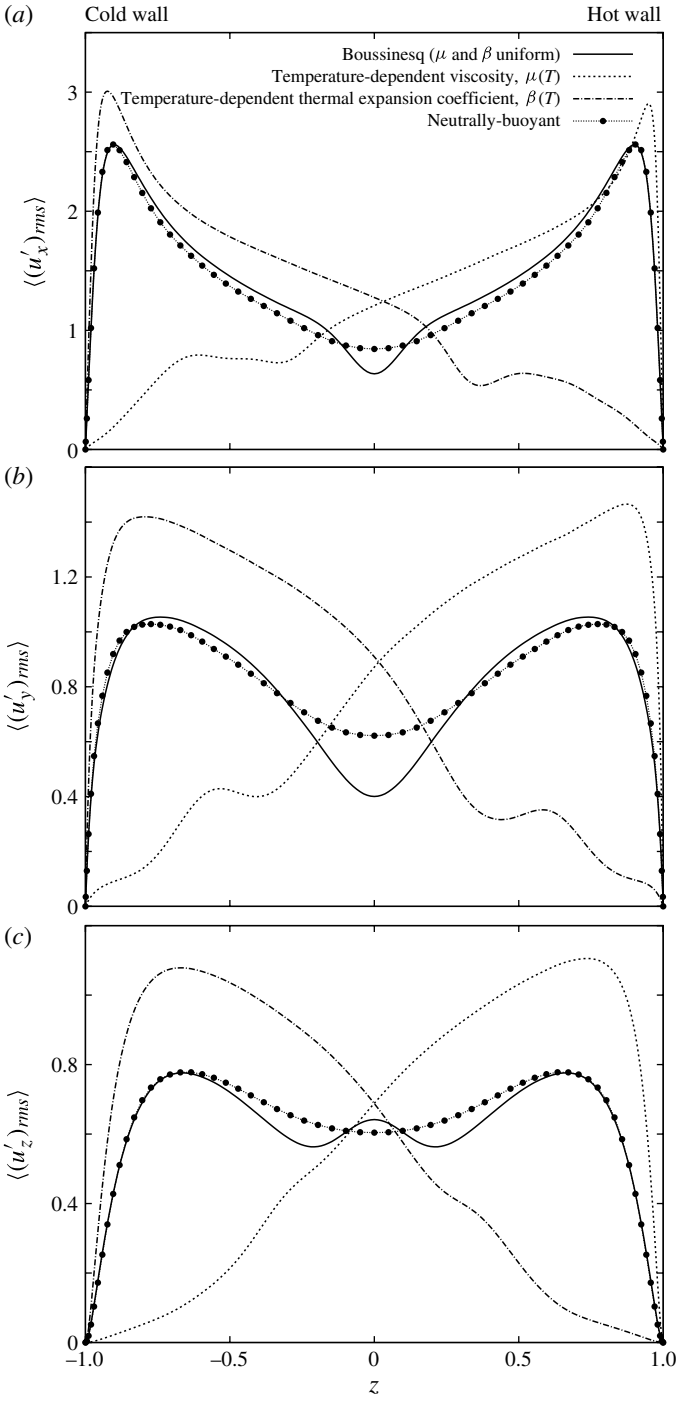

FIGURE 5. Root mean square (r.m.s.) of fluid velocity fluctuations for stably-stratified turbulent channel flow at $Ri_\tau = 498$ ($Re_\tau = 150$): (*a*) streamwise component, $\langle (u_x')_{rms} \rangle$; (*b*) spanwise component, $\langle (u_y')_{rms} \rangle$; (*c*) wall-normal component, $\langle (u_z')_{rms} \rangle$. Lines as in figure 4.

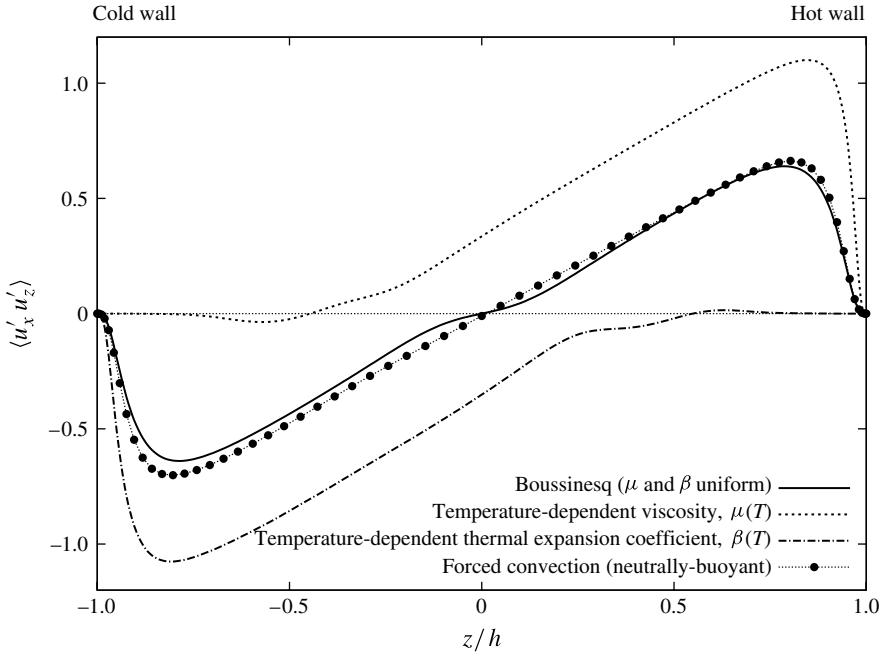

FIGURE 6. Turbulent shear stress, $\langle u_x' u_z' \rangle$, for stably-stratified turbulent channel flow at $Ri_\tau = 498$ ($Re_\tau = 150$). Lines as in figure 4.

The temperature-dependent viscosity (dotted line) alters the symmetry of the profiles. Turbulence intensities are suppressed near the cold wall and enhanced near the hot wall, according to the viscosity distribution across the channel: where viscosity is lower (hot wall) turbulence is promoted, and where viscosity is higher (cold wall) turbulence is damped. The selective turbulence modulation induced by viscosity produces a flow configuration in which turbulence exists only near the hot wall ($0 < z < 1$), although near the cold wall ($-1 < z < 0$) the flow relaminarizes.

An opposite situation occurs when the temperature-dependent thermal expansion coefficient (dash-dotted line) is considered. In this case, velocity fluctuations are increased near the cold wall, and decreased near the hot wall, insomuch as turbulence is sustained only near the cold wall ($-1 < z < 0$). To analyse further the mechanism of turbulence modification by buoyancy, we compute the turbulent shear stresses $\langle u_x' u_z' \rangle$ (figure 6). Upon comparison between the case of stable stratification with uniform thermophysical properties (solid line) and neutrally-buoyant flow (symbols), we note that stable stratification generally reduces turbulence (reduction of $\langle u_x' u_z' \rangle$). The mechanism of turbulence suppression is simple: first, the buoyancy force extracts energy directly from the wall-normal component of the velocity, reducing $\langle u_x' u_z' \rangle$. Then, the interaction of $\langle u_x' u_z' \rangle$ with the mean velocity gradient contributes directly to the u_x component of the turbulent kinetic energy. Finally, energy is redistributed to the u_y and u_z components by the action of pressure fluctuations (Arya 1975). As expected, the effect of temperature-dependent viscosity and thermal expansion coefficient on $\langle u_x' u_z' \rangle$ is important. In the case of temperature-dependent viscosity (dotted line) $\langle u_x' u_z' \rangle$ is suppressed near the cold wall and enhanced near the hot wall. This indicates that the viscous stress (not shown for brevity) is very important near the cold wall (zone of

laminarization) but less important near the hot wall. The opposite situation occurs in the case of temperature-dependent thermal expansion coefficient (dash-dotted line).

Results obtained from simulations with temperature-dependent thermal expansion coefficient may be explained with simple physical arguments. The buoyancy force acting on a fluid particle is proportional to the local value of the thermal expansion coefficient, $F_B \sim \beta(z)$ (with straightforward meaning of the symbols). The ratio of the buoyancy force between the cold (labelled C) and the hot wall (labelled H) is $F_{B,r} \sim \beta_C/\beta_H$: the larger the deviation of $F_{B,r}$ from unity, the larger the asymmetry due to temperature-dependent thermal expansion coefficient. In our case, $F_{B,r} < 1$, meaning that the hot wall (placed above) produces more upward buoyancy than the downward buoyancy produced by the cold surface (placed below). Therefore, a fluid parcel close to the hot wall will experience a positive buoyancy larger than the negative buoyancy experienced by a fluid parcel close to the cold wall. To the best of our knowledge, one-sided turbulent channel flows have not been observed experimentally. However, they have been observed in numerical simulations of both stratified (Iida *et al.* 2002; Lessani & Zainali 2009) and unstratified channel flows (Herbert 1983; Saiki *et al.* 1993).

4.2.2. *Fluid temperature statistics*

In figure 7(*a*) the mean temperature profiles from simulations of stable stratification ($Ri_\tau = 498$, $Re_\tau = 150$) with uniform and temperature-dependent fluid properties are shown and compared with that from the corresponding neutrally-buoyant simulation. Stable stratification (solid line) has a twofold effect on the temperature field compared to the neutrally-buoyant case (symbols): it reduces the temperature gradient at the wall (i.e. the Nusselt number) and at the same time it increases the temperature gradient in the core of the channel. In particular, the increased temperature gradient in the core of the channel indicates a tendency to form a kind of thick interface in this region. This interface, in which temperature changes more rapidly with depth than it does in the regions above or below, is usually called a *thermocline* (see § 4.3 for details). The influence of temperature-dependent viscosity (dotted line) is evident. Near the cold wall ($-1 < z < -0.7$), where the flow is laminar, the mean temperature profile is roughly linear. Near the hot wall, where turbulence is sustained, the mean temperature profile is flat. This suggests that heat is efficiently transferred by wall-normal velocity fluctuations (see § 4.2.1) away from the hot wall, but less efficiently transferred towards the cold wall. A reversed situation is observed for temperature-dependent thermal expansion coefficient (dash-dotted line). In this case, the mean temperature profile is roughly linear near the hot wall and flat near the cold wall. This behaviour is a direct consequence of the sharp separation of the channel into a laminar zone (near the hot wall) and a turbulent zone (near the cold wall).

The root mean square of temperature fluctuations is shown in figure 7(*b*). Compared to the neutrally-buoyant case (symbols), we observe that the peak value moves from the near-wall region towards the central region of the channel. However, fluctuations in the core region of the channel may be associated with large-scale wavy motions (IGW) rather than with turbulence structures. The temperature-dependent viscosity produces a general attenuation of temperature fluctuations throughout the channel. In this case, the peak value of $\langle (T')_{rms} \rangle$ is shifted towards the cold wall, indicating that internal waves lie in the cold side of the channel rather than being located near the centreline (see § 4.3 for details). When the temperature-dependent thermal expansion coefficient is considered, the situation reverses, and the peak of temperature fluctuations (i.e. the maximum wave activity) moves towards the hot wall.

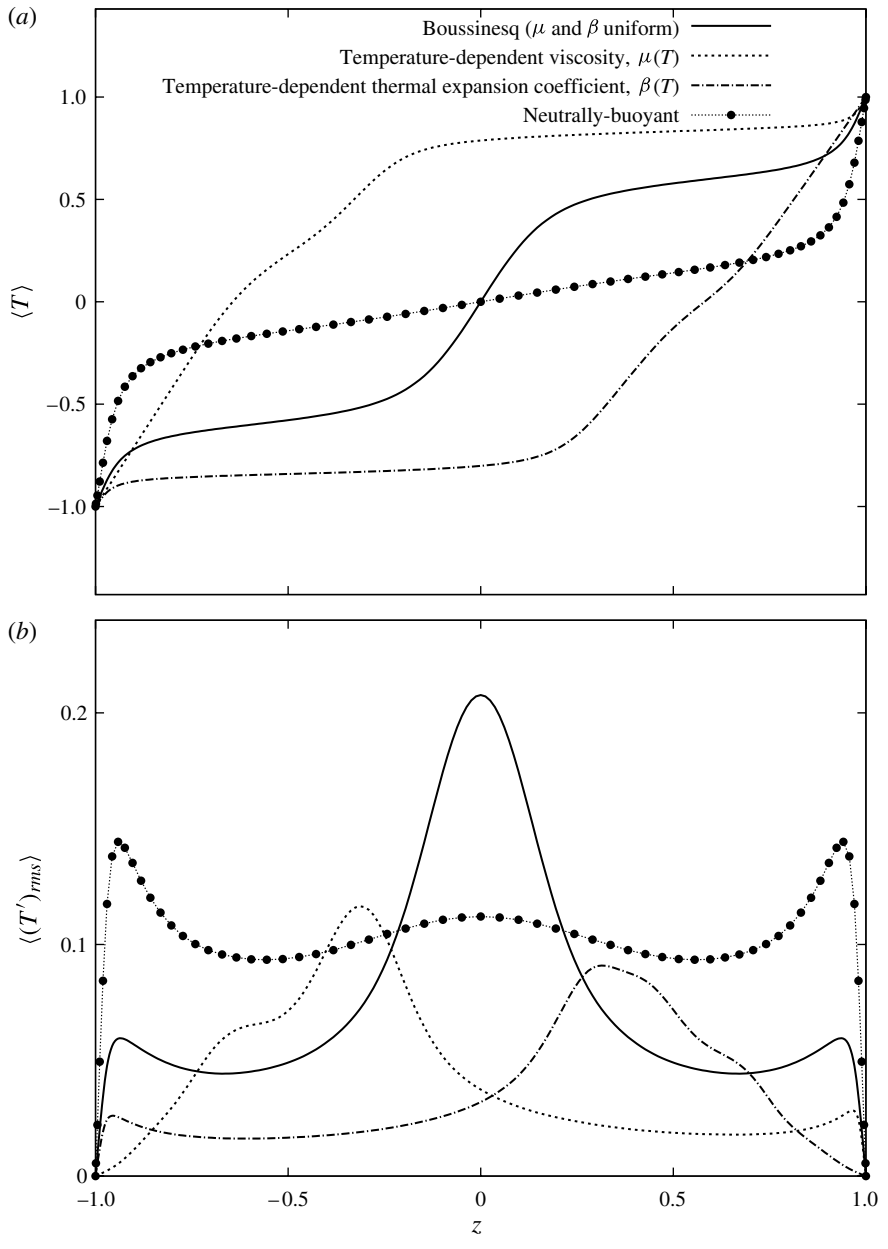

FIGURE 7. Fluid temperature statistics for stably-stratified turbulent channel flow at $Ri_\tau = 498$ ($Re_\tau = 150$): (*a*) mean fluid temperature, $\langle T \rangle$; (*b*) root mean square of temperature fluctuations, $\langle (T')_{rms} \rangle$. Lines as in figure 4.

4.3. *Internal waves in stably-stratified turbulent channel flow*

Visualizations of the flow structures are presented and discussed to gain insights into the phenomena responsible for the results presented in the previous section. The simplest way to identify internal waves is by using contour maps of the temperature field: temperature is advected by velocity and reproduces faithfully the underlying

structure of the flow field (internal waves can be detected). In figure 8 contour maps of the temperature field for simulations of stable stratification at $Ri_\tau = 498$ with uniform (figure 8*a*) and temperature-dependent (figure 8*b,c*) fluid properties are shown. Three-dimensional (greyscale) views and associated bidimensional (black and white) sections are combined to highlight the fundamental features of internal waves. In figure 8(*a*) we consider the base simulation with uniform thermophysical properties. It is clear that turbulence and internal waves coexist. In particular, internal waves (moving from left to right) are found in a narrow region of the channel around the centreline, whereas intermittent bursts associated with turbulence characterize the near-wall region. The region where internal waves are observed coincides with the region where a thermocline exists (see figure 7), proving that internal waves may be produced in a thermocline (Ferziger, Koseff & Monismith 2002). Mixing efficiency is strongly influenced by this thermocline: the fluid parcels that reach the thermocline do not have enough energy to penetrate it, since the thermocline is a kind of thick interface. As a result, the process that produces mixing is different. In a neutrally-buoyant flow, mixing is achieved first by parcels of high-temperature fluid begin enveloped by the low-temperature fluid, and later by diffusion of fluids across their separation interface. In a stably-stratified flow, parcels of high temperature are scoured off the interface. There is no enveloping of large parcels of fluid, and mixing is reduced considerably.

In figure 8(*b*) we focus on stable stratification with temperature-dependent viscosity. A strong asymmetry in the structure of the flow field is observed. The flow is laminar at the cold side of the channel (where viscosity is higher), but remains turbulent at the hot side (where viscosity is lower). In this situation, the thermocline (and the associated internal waves) moves towards the cold wall and extends over a larger proportion of the channel (more than 1/3 of the entire height of the channel).

The situation reverses in figure 8(*c*), where the effect of the temperature-dependent thermal expansion coefficient is considered. In this case, flow laminarization occurs at the hot side of the channel, where the thermal expansion coefficient is higher. Note that the thermocline and the associated internal waves move accordingly towards the hot side of the channel.

Results of flow laminarization on one side of the domain for temperature-dependent fluid properties may also be explained with simple scaling arguments. In the case of temperature-dependent viscosity, the local Reynolds number (which depends on viscosity) is lower near the cold wall, and higher near the hot wall. The corresponding local Richardson number ($Ri_\tau = Gr/Re_\tau^2$) increases near the cold wall and decreases near the hot wall, meaning that stratification is stronger (higher Ri_τ) near the cold wall (where local laminarization occurs), and weaker near the hot wall. In the case of temperature-dependent thermal expansion coefficient, the local Grashof number (which depends on the thermal expansion coefficient) is higher near the hot wall and lower near the cold wall. The corresponding local Richardson number ($Ri_\tau = Gr/Re_\tau^2$) is higher near the hot wall and lower near the cold wall, meaning that stratification is stronger (higher Ri_τ) near the hot wall (where local laminarization occurs), and weaker near the cold wall.

The asymmetric behaviour of the flow field in the case of temperature-dependent fluid properties is visualized in figure 9 by isosurfaces of temperature distribution. Note that the computational domain has been turned upside-down in figures 9(*a*) and 9(*c*) (hot wall below) for visualization purposes (the z axis is shown explicitly beside each figure). In case of temperature-dependent viscosity (figure 9*a,b*), the isosurface near the hot wall, $T = 0.7$ (light grey), is more energetically destroyed, indicating that the temperature field is effectively mixed by turbulent motions. By contrast, the

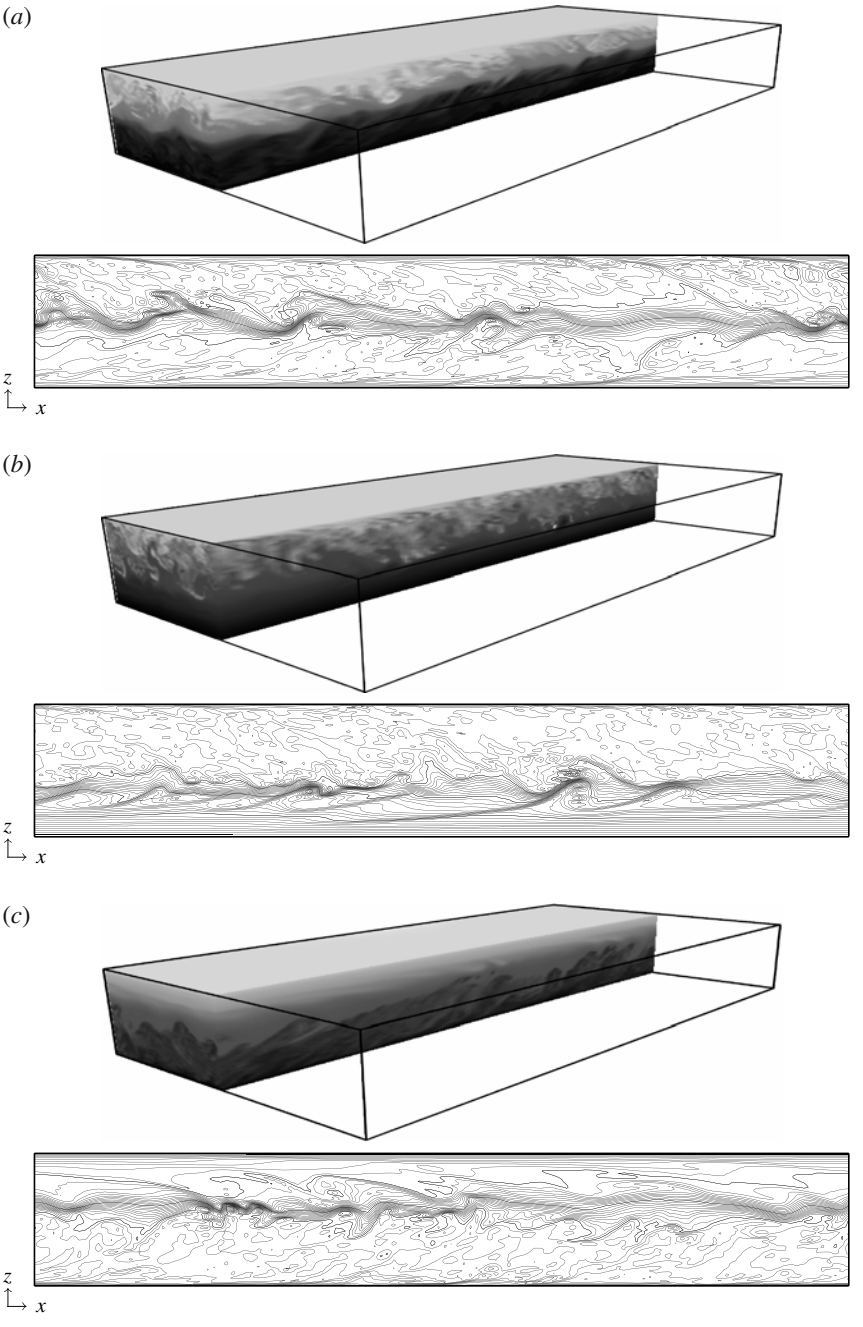

FIGURE 8. Contour maps of the temperature field for simulations at $Ri_\tau = 498$ ($Re_\tau = 150$) after the steady-state condition has been reached. Three-dimensional visualizations of temperature distribution and associated two dimensional views (x–z planes, black and white) are shown: (*a*) uniform thermophysical properties; (*b*) temperature-dependent viscosity; (*c*) temperature-dependent thermal expansion coefficient.

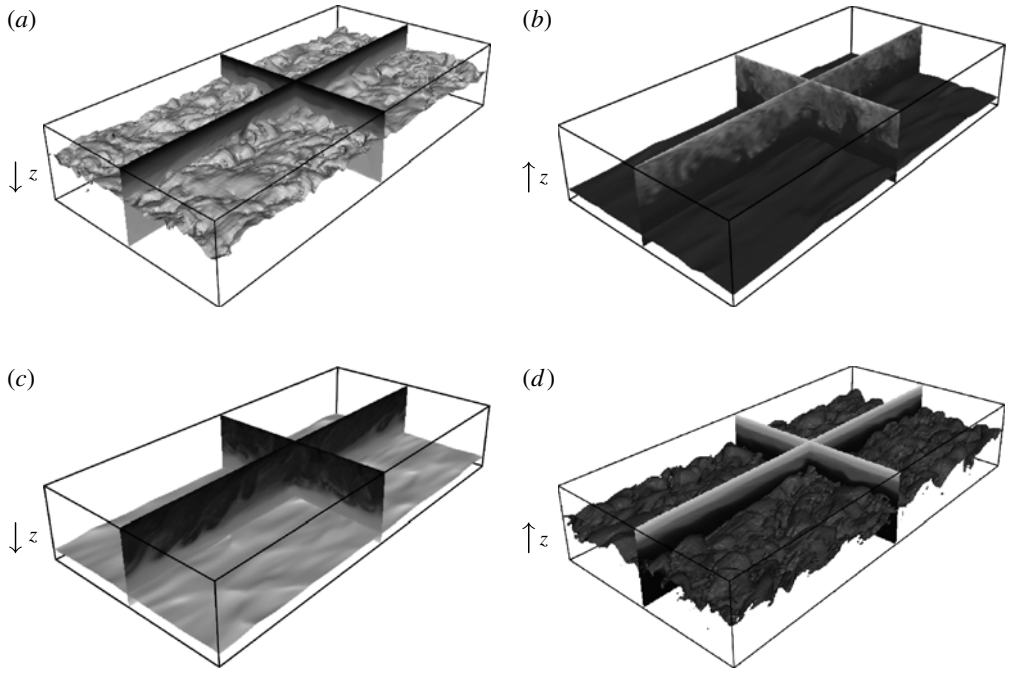

FIGURE 9. Isosurfaces of temperature field (and associated temperature contours on x–z and y–z planes) for stably-stratified turbulent channel flow at $Ri_\tau = 498$ ($Re_\tau = 150$). Comparison between the shape of temperature isosurfaces in the hot and cold sides of the channel for simulations with temperature-dependent viscosity and temperature-dependent thermal expansion coefficient: (*a*) $T = 0.7$, temperature-dependent viscosity; (*b*) $T = -0.7$, temperature-dependent viscosity; (*c*) $T = 0.7$, temperature-dependent thermal expansion coefficient; (*d*) $T = -0.7$, temperature-dependent thermal expansion coefficient. Note that the domains in (*a*) and (*c*), for $T = 0.7$, are upside down.

temperature isosurface near the cold wall, $T = -0.7$ (dark grey) exhibits smaller undulations, according to the reduced wall-normal mixing caused by higher values of viscosity. The opposite situation, with larger fluctuations in the cold side of the channel than in the hot side, is found for temperature-dependent thermal expansion coefficient (figure 9*c,d*).

4.4. *Buoyancy frequency and the gradient Richardson number*

Stratified flows can support a variety of types of wave motions which cannot be observed in non-stratified flows. The reason is the tendency for wall-normal motion (the gravitational acceleration acting along the wall-normal direction) to be suppressed: a fluid particle that does get displaced in the wall-normal direction tends to be restored to its original position; it may overshoot inertially and oscillate about this position. The characteristic frequency of oscillation is called buoyancy frequency (or Brunt–Väisälä frequency) and can be computed as

$$N^* = \left(g^* \beta^*(z) \frac{\mathrm{d}T_0^*}{\mathrm{d}z^*} \right)^{1/2}, \tag{4.1}$$

with T_0^* the temperature of the fluid particle. In figure 10(*a*) the dimensionless buoyancy frequency, $N = N^* h^* / u_\tau^*$, is shown for simulations of stable stratification

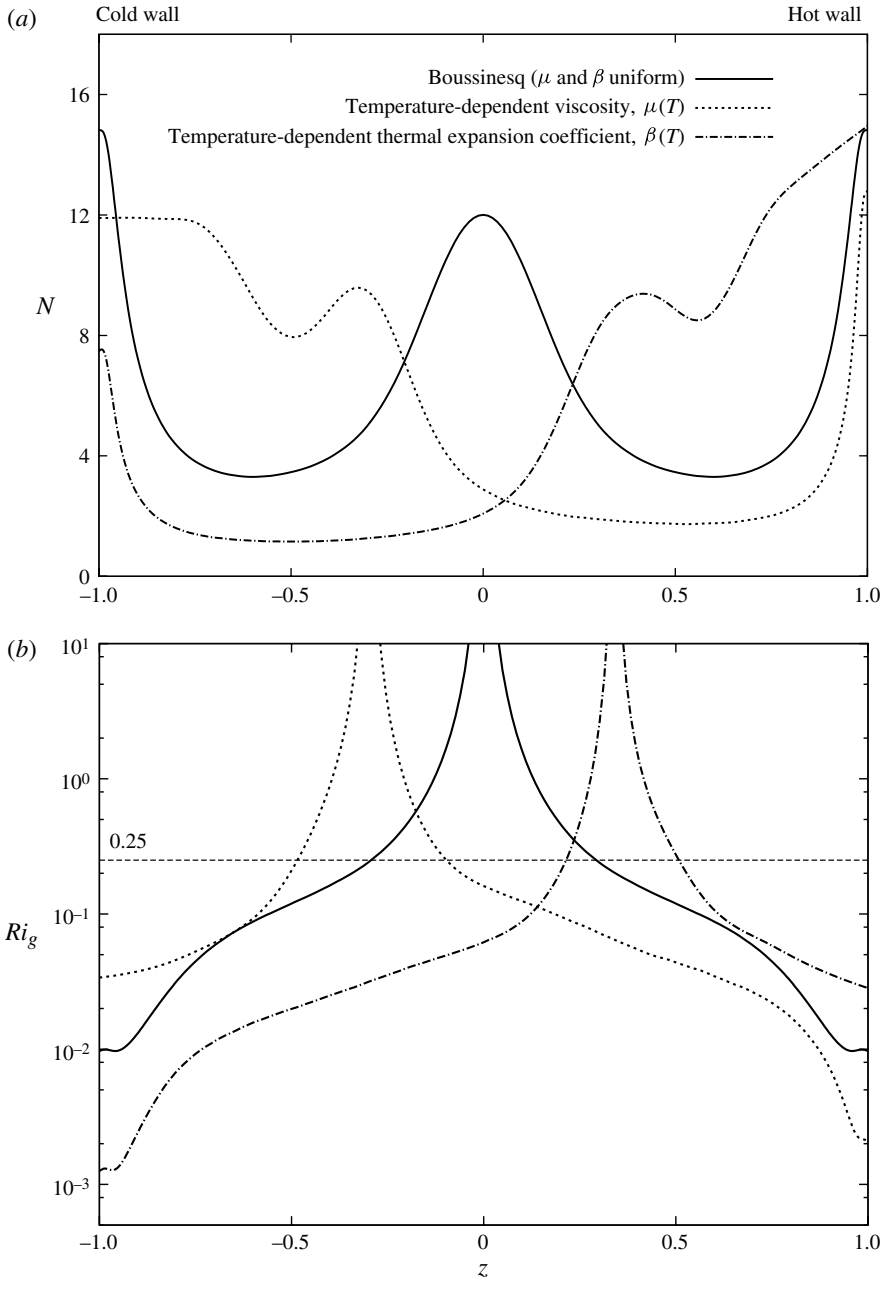

FIGURE 10. Stably stratified turbulent channel flow at $Ri_\tau = 498$ ($Re_\tau = 150$): (*a*) buoyancy frequency, N; (*b*) gradient Richardson number, Ri_g. Lines as in figure 4.

at $Ri_\tau = 498$ ($Re_\tau = 150$) with uniform and temperature-dependent fluid properties. For uniform fluid properties (solid line), N decreases rapidly in the wall layer and is nearly constant in the core of the channel, except for a narrow region near the centre of the channel, where wave activity is observed (Saiki, Moeng & Sullivan 2000; Armenio & Sarkar 2002). Such a profile is directly linked to the sharpening of

the mean temperature profile in the centre of the channel (figure 7). In the case of temperature-dependent viscosity (dotted line), the influence of internal waves extends over a wider region, from the centre of the channel up to the cold wall ($-1 < z < 0$). This result quantifies the observation made in § 4.3 that internal waves in the case of temperature-dependent viscosity are shifted towards the cold wall and extend over a large proportion of the cold side of the channel. A reversed situation occurs in the case of temperature-dependent thermal expansion coefficient (dash-dotted line), with larger values of N in a region between the centreline of the channel and the hot wall. This corresponds to the wave activity observed in the hot side of the channel (see figure 8*c*). Note that the maximum of N for the cases of temperature-dependent fluid properties roughly coincides with that for the case of uniform thermophysical properties, the only difference being the position (z) at which the maximum occurs.

The buoyancy frequency is useful to compute the gradient Richardson number,

$$Ri_g = \frac{N^2}{S^2} = \frac{g\beta(z)\dfrac{\mathrm{d}\langle T\rangle}{\mathrm{d}z}}{\left(\dfrac{\mathrm{d}\langle u_z\rangle}{\mathrm{d}z}\right)^2}. \tag{4.2}$$

The gradient Richardson number has been extensively used as the key parameter in uniformly sheared flows with linear stratification because of the spatially constant value of Ri_g. Results from homogeneous flows subject to thermal stratification (Rohr *et al.* 1988; Holt, Koseff & Ferziger 1992) reveal that when $Ri_g \simeq 0.25$ the turbulence neither grows nor decay. At lower Richardson numbers turbulence grows, whereas at higher ones it decays.

In wall-bounded flows, the spatial inhomogeneity of the flow forces the gradient Richardson number to vary along the wall-normal coordinate (Armenio & Sarkar 2002; Taylor, Sarkar & Armenio 2005). Profiles of the local values of the gradient Richardson number Ri_g are shown in figure 10(*b*). It is very large where $\mathrm{d}\langle u_z\rangle/\mathrm{d}z \to 0$ (and singular where $\mathrm{d}\langle u_z\rangle/\mathrm{d}z = 0$), whereas it is below 0.1 in a large region near the walls. The behaviour of the gradient Richardson number can be useful to classify the regions of turbulent and non-turbulent states. Where Ri_g exceeds 0.25 (horizontal dashed line in figure 10*b*), turbulence is significantly attenuated and internal waves are the dominant flow structures. As expected, the profile of Ri_g suggests that internal waves lie: (i) near the centreline of the channel for uniform fluid properties (solid line); (ii) in the cold side of the channel for temperature-dependent viscosity (dotted line); and (iii) in the hot side of the channel for temperature-dependent thermal expansion coefficient (dash-dotted line).

4.5. *Frequency spectra*

To study the effect of buoyancy and temperature-dependent thermophysical properties on eddy sizes, we measured the streamwise energy spectra of velocity and temperature fluctuations (Iida *et al.* 2002; Yeo, Kim & Lee 2009). In particular, in figure 11 we consider the streamwise energy spectra of the wall-normal velocity fluctuations ($u_z'^2$) at three different positions (expressed in wall units, $z^+ = z^* u_\tau^* / \nu_{ref}^*$) along the wall-normal direction. For each position, results from the simulation with uniform thermophysical properties (filled circles) are compared with those with temperature-dependent viscosity (filled triangles) and temperature-dependent thermal expansion coefficient (filled squares). Results from simulation of neutrally-buoyant flow (open circles) are also shown for comparison purposes.

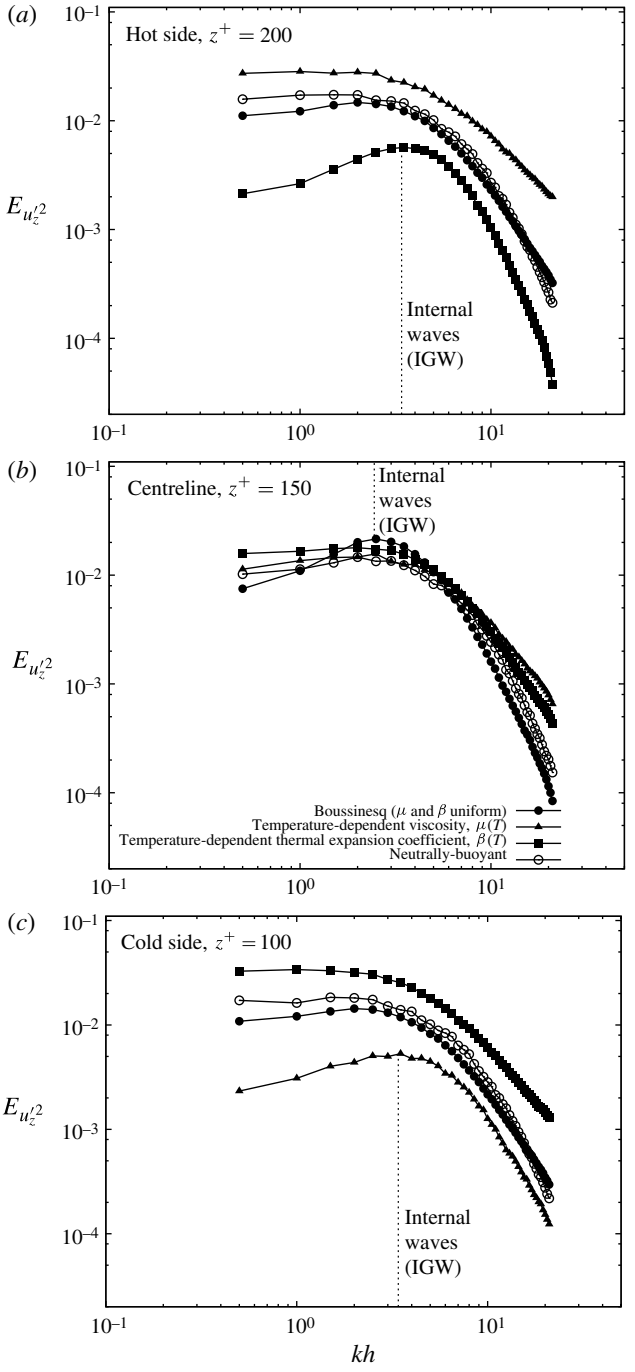

FIGURE 11. Streamwise frequency spectra of wall-normal velocity fluctuations ($Ri_\tau = 498$) at three different positions along the wall normal direction: (*a*) $z^+ = 200$ (hot side); (*b*) $z^+ = 150$ (centreline); (*c*) $z^+ = 100$ (cold side). Comparison between simulations with uniform thermophysical properties (filled circles) and with temperature-dependent viscosity (filled triangles) and temperature-dependent thermal expansion coefficient (filled squares). Results from simulation of neutrally-buoyant turbulent channel flow (open circles) are also included.

Effects induced purely by stratification can be inferred by comparison between results from simulations of neutrally-buoyant flow (open circles) and stable stratification with uniform thermophysical properties (filled circles). The energy spectra outside the core region (figures 11*a* and 11*c*) decrease at low wavenumbers, indicating that turbulent scales are selectively modified by buoyancy, with a maximum impact on larger and slower structures of the flow (low wavenumbers). In the core region of the channel (figure 11*b*), the energy spectrum increases for $1 < kh < 4$, with a peak value for $kh \simeq 2.5$ (where k is wavenumber). This is the footprint of internal waves which induce fluctuations of wall-normal velocity (u_z') occurring at the characteristic frequency of the wave. We demonstrate this correlation using simple arguments. We assume that internal waves move with a velocity similar to the fluid velocity at the centreline ($u^+_{wave} \simeq 24$, see figure 4). The associated frequency is $f_{wave} = u_{wave} \times k/2\pi \simeq 15\ \mathrm{s}^{-1}$ (where $u_{wave} = u^+_{wave} \times u_\tau$). The buoyancy frequency in the core region of the channel ($-0.3 < z < 0.3$) ranges between $10 \leqslant N^* \leqslant 25\ \mathrm{s}^{-1}$ ($5 \leqslant N \leqslant 12$, see figure 10*a*), in fair agreement with the previous calculation.

Unlike the case of uniform thermophysical properties, the effect of temperature-dependent viscosity (filled triangles) is higher outside the core region of the channel. Interestingly, in the cold side of the channel (figure 11*c*) the energy spectrum exhibits a non-monotonic behaviour with an initial increase (up to $kh \simeq 3.5$) followed by a sharp decrease ($kh > 3.5$). This behaviour is induced by internal waves lying in the cold side of the channel (see also figure 8*b*). In the case of temperature-dependent thermal expansion coefficient (filled squares), the energy spectrum exhibits a non-monotonic behaviour in the hot side of the channel (figure 11*a*), where wave activity was observed (see also figure 8*c*).

5. Conclusions

Stably-stratified turbulence is characterized by complex macroscopic phenomena that are rich in physics yet difficult to model and/or to reproduce. Complexity grows in situations where the thermophysical properties of the fluid depend strongly on temperature. This is the case of water flows, in which the occurrence of large temperature gradients produces significant variations of fluid properties. In this paper, we focus on the effects produced by a temperature-dependent viscosity and thermal expansion coefficient on a stably-stratified turbulent channel flow. To study these effects, we performed a numerical experiment based on an extensive campaign of direct simulations of heat transfer in a stably-stratified turbulent channel flow with water as working fluid. Simulations are based on a numerical methodology tailored to the time-accurate integration of momentum and energy equations written in their variable-viscosity/thermal expansion coefficient formulation.

Turbulent channel flow simulations (with uniform and with temperature-dependent fluid properties) were run at Prandtl number $Pr = 3$ and shear Richardson numbers $Ri_\tau = 926$, 498 and 346 (corresponding to shear Reynolds numbers $Re_\tau = 110$, 150, 180 and Grashof number $Gr = 1.12 \times 10^7$). The transient evolution of an initially turbulent neutrally-buoyant channel flow reveals a two-stage process made of: (i) a first transition from turbulent to laminar flow; and (ii) a return transition to turbulence, depending on the value of the Richardson number. For the largest stratification level considered in this study, $Ri_\tau = 926$ (and $Re_\tau = 110$), a steady-state laminar condition is observed (a return transition to turbulence does not occur). The statistical moments for the fluid velocity and temperature fields obtained from simulations with uniform and temperature-dependent fluid properties have been compared to those from

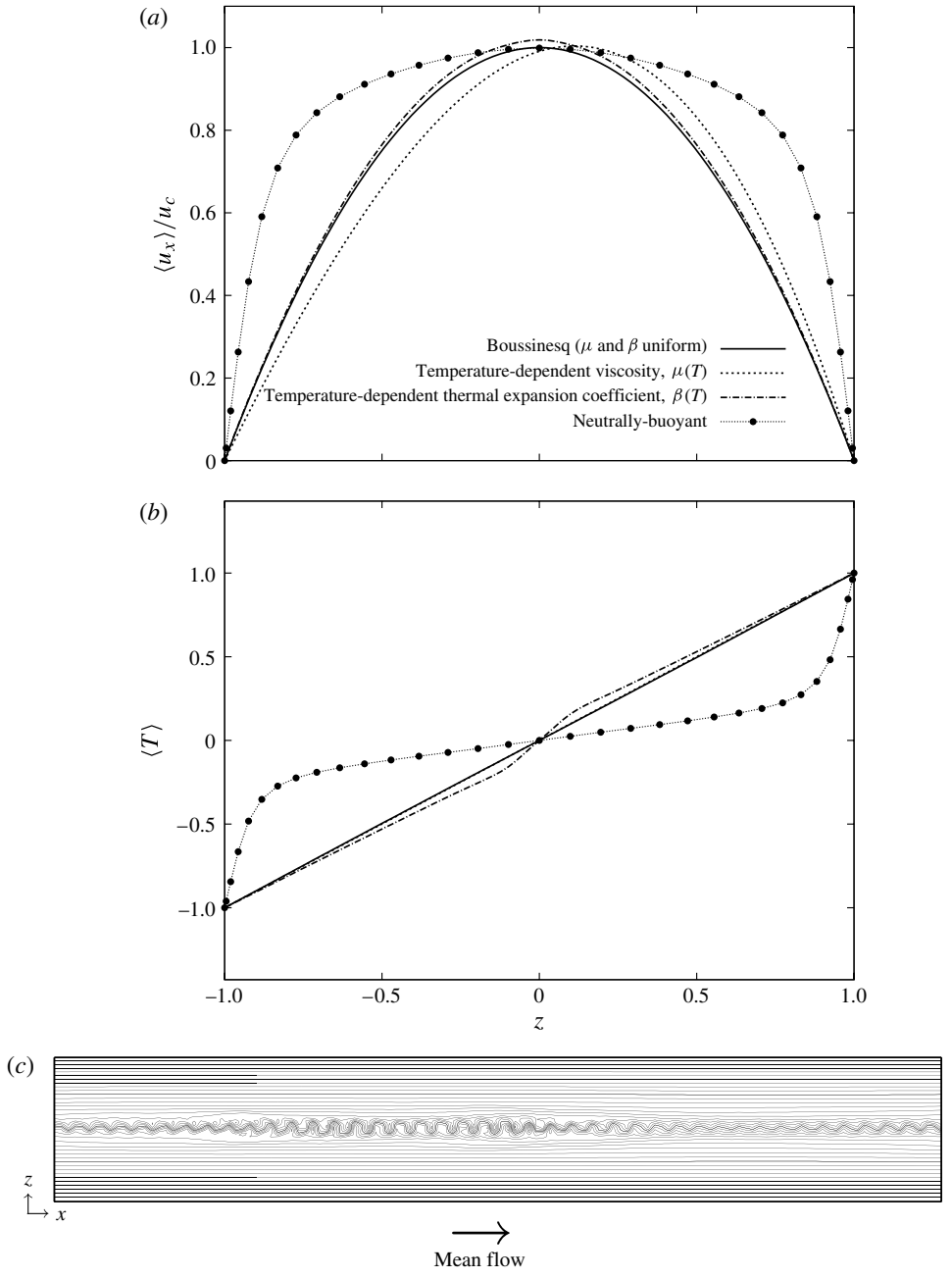

FIGURE 12. Results from simulation of stably-stratified channel flow at $Ri_\tau = 926$ ($Re_\tau = 110$). (*a*) Mean fluid streamwise velocity $\langle u_x \rangle / u_c$; (*b*) mean fluid temperature $\langle T \rangle$ (lines as in figure 4). (*c*) Flow structures (visualized using temperature contours on an x–z plane) for the simulation with temperature-dependent thermal expansion coefficient.

neutrally-buoyant simulations. Discussion referred to the simulations at $Re_\tau = 150$. Stable stratification suppresses the wall-normal transport of momentum and heat compared to the neutrally-buoyant case, where temperature is a passive scalar.

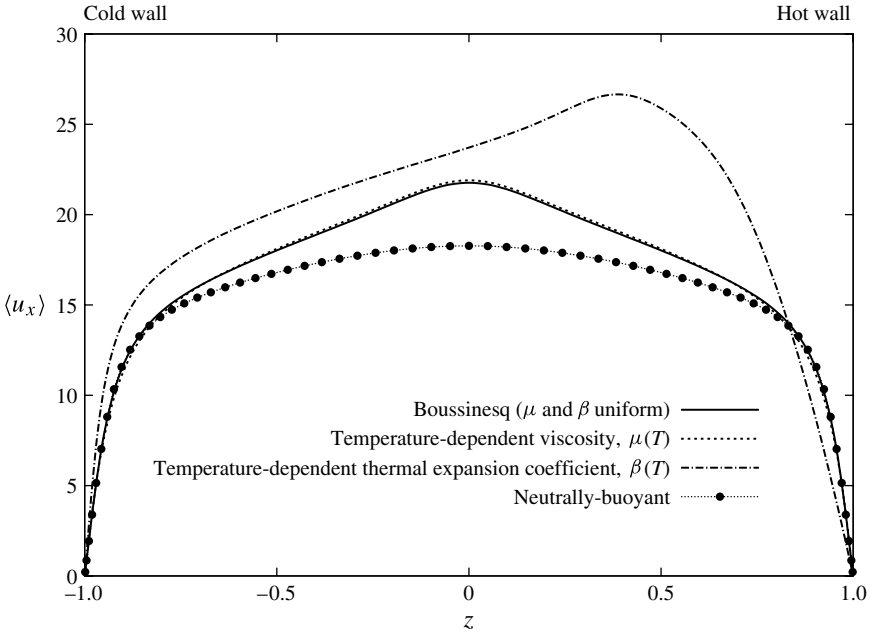

FIGURE 13. Mean fluid streamwise velocity $\langle u_x \rangle$ for stably-stratified turbulent channel flow at $Ri_\tau = 346$ ($Re_\tau = 180$). Lines as in figure 4.

Instantaneous realizations of the flow field show that internal gravity waves (IGW) and active turbulence coexist. The role of temperature-dependent fluid properties has been found to be extremely important and the cause of large flow asymmetries. In the case of temperature-dependent viscosity, local flow laminarization occurs in the cold side of the channel (where viscosity is higher) whereas active turbulence persists in the hot side of the channel (where viscosity is lower). The situation reverses in the case of temperature-dependent thermal expansion coefficient, with local flow laminarization occurring in the hot side of the channel. We have justified these observations with scaling arguments based on local values of viscosity and thermal expansion coefficient.

We have also provided a qualitative explanation of the observed statistical behaviour by examining the instantaneous flow structure (contour maps of the temperature field). These instantaneous visualizations have shown the asymmetric behaviour of the flow, with local laminarization occurring either at the cold side (for temperature-dependent viscosity) or at the hot side (for temperature-dependent thermal expansion coefficient) of the channel. To explore further, we have computed frequency spectra of the wall-normal velocity fluctuations at three different positions along the wall-normal direction. We have found that turbulence is generally attenuated at low wavenumbers while it is strengthen at high wavenumbers. In some cases, frequency spectra have a non-monotonic behaviour with a visible peak: this is the footprint of internal waves.

The impact of temperature-dependent fluid properties on the behaviour of the flow field depends on the value of the Reynolds (or Richardson) number. At lower Reynolds numbers ($Re_\tau = 110$ in this work) the effects of temperature-dependent viscosity are more important than the effects of temperature-dependent thermal expansion coefficient. At higher Reynolds numbers ($Re_\tau = 180$ in this work) the situation reverses and the effects of temperature-dependent thermal expansion coefficient are larger than the effects of temperature-dependent viscosity. There is

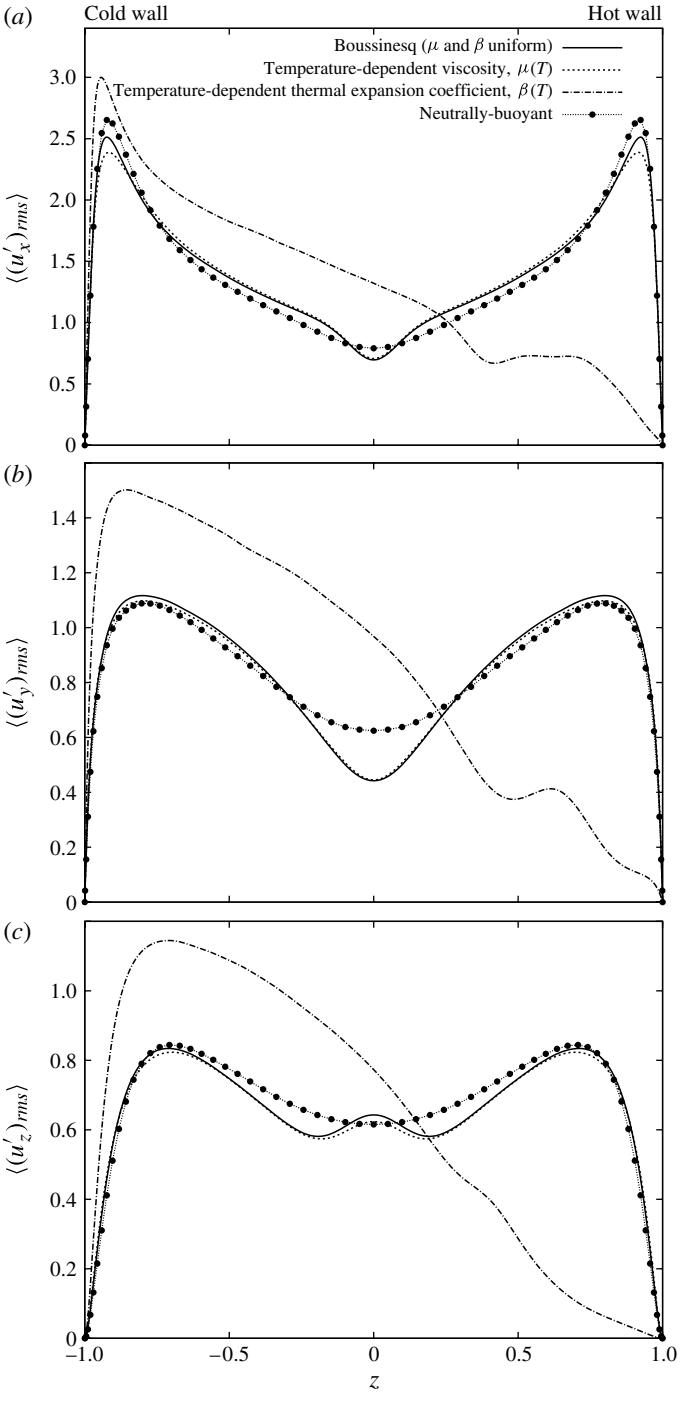

FIGURE 14. Root mean square (r.m.s.) of fluid velocity fluctuations for stably-stratified turbulent channel flow at $Ri_\tau = 346$ ($Re_\tau = 180$): (*a*) streamwise component, $\langle (u'_x)_{rms} \rangle$; (*b*) spanwise component, $\langle (u'_y)_{rms} \rangle$; (*c*) wall-normal component, $\langle (u'_z)_{rms} \rangle$. Lines as in figure 4.

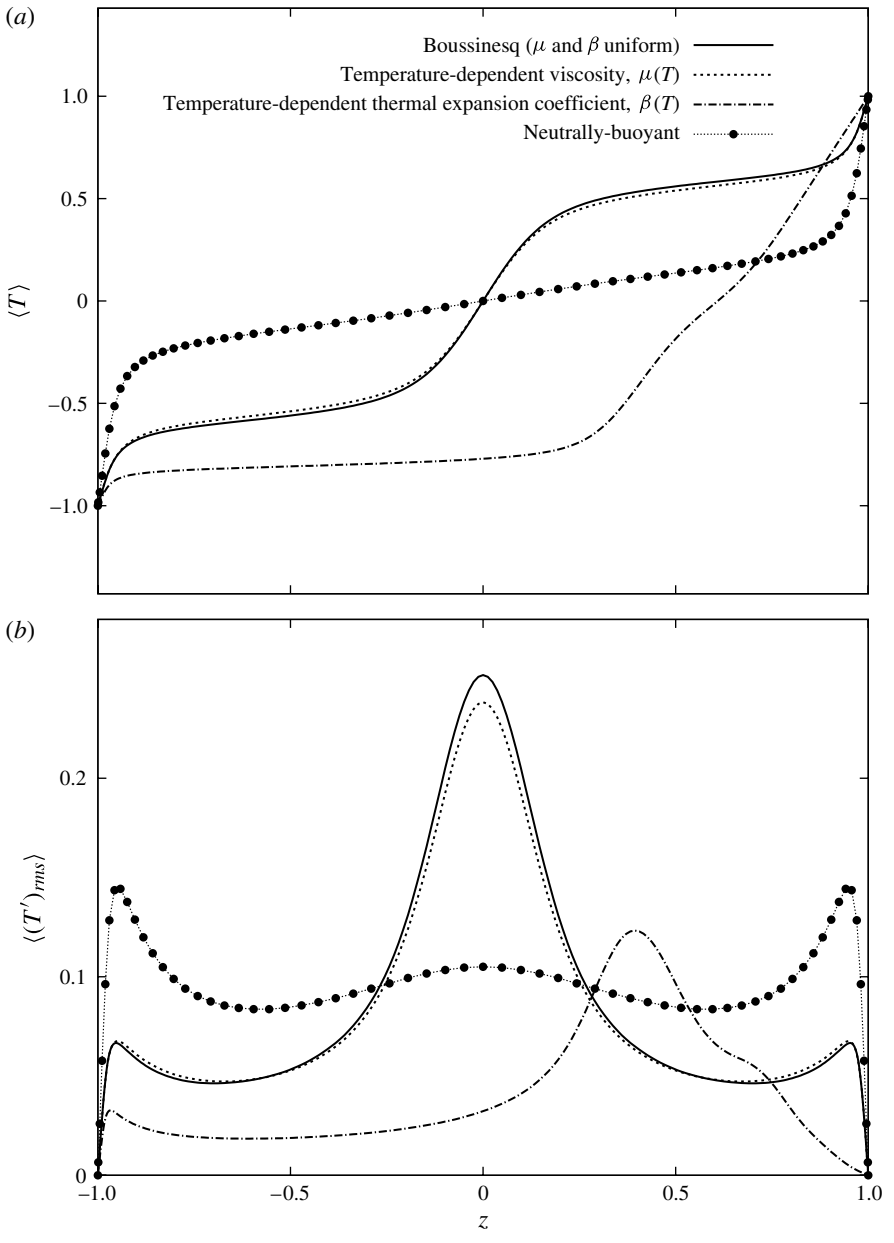

FIGURE 15. Fluid temperature statistics for stably-stratified turbulent channel flow at $Ri_\tau = 346$ ($Re_\tau = 180$): (*a*) mean fluid temperature, $\langle T \rangle$; (*b*) root mean square of temperature fluctuations, $\langle (T')_{rms} \rangle$. Lines as in figure 4.

a range of intermediate situations ($Re_\tau = 150$ in this work) in which these effects are of comparable order. In this case, variations of viscosity and thermal expansion coefficient (with temperature) are both of fundamental importance. None of these effects can be neglected for accurate prediction of stably-stratified turbulent channel flows subject to large temperature gradients.

Acknowledgements

CINECA supercomputing centre (Bologna, Italy) and DEISA Extreme Computing Initiative are gratefully acknowledged for generous allowance of computer resources. Support from PRIN (under grant 2006098584_004) and from HPC Europa Transnational Access Program (under grants 466 and 708) are gratefully acknowledged. F.Z. gratefully acknowledges the Department of Physics, University of Torino, for financial support under grant 234175.

Appendix. Fluid statistics for $Ri_\tau = 926$ and $Ri_\tau = 346$

In § 4.2 we analysed carefully the statistics of stably-stratified turbulence at $Ri_\tau = 498$. Here, we present the results of computations performed at $Ri_\tau = 926$ and $Ri_\tau = 346$.

A.1. *Case I:* $Ri_\tau = 926$

In figure 12(*a*) the mean axial velocity profiles $\langle u_x \rangle / u_c$ (u_c being the centreline velocity) for the case of stable stratification at $Ri_\tau = 926$ are shown as a function of the dimensionless wall-normal coordinate z. Profiles are parabolic, suggesting that a steady-state laminar condition with a complete suppression of turbulence occurs. This is also revealed by the mean temperature profile (figure 12*b*), which is a straight line between the fixed values of temperature at $z = -1$ and $z = 1$. The role of temperature-dependent fluid properties is relatively less important. The temperature-dependent viscosity (dotted line) skews the mean velocity profile, but the flow remains laminar. The temperature-dependent thermal expansion coefficient (dash-dotted line) produces only a slight increase of the mean axial velocity. However, a careful analysis of figure 12(*b*) reveals that a mild wave activity persists in the core region of the channel (note the different slope of the mean temperature profile). This is clearly visualized in figure 12(*c*) through a contour map of the temperature field on an x–z plane.

A.2. *Case II:* $Ri_\tau = 346$

In figures 13–15 we considered the fluid statistics for the case of stable stratification at $Ri_\tau = 346$. Results are qualitatively similar to those discussed in § 4.2 for $Ri_\tau = 498$. The main difference is limited to the role of temperature-dependent viscosity. In this case, its effect is almost negligible, since profiles (dotted line) collapse onto those from a simulation with uniform thermophysical properties. The role of temperature-dependent thermal expansion coefficient is on the other hand very important, and it is qualitatively similar to that observed in § 4.2.

These considerations suggest that the role of temperature-dependent fluid properties is non-monotonic. At lower Reynolds number (and higher Richardson number), effects induced by the temperature-dependent viscosity are more important than effects induced by the temperature-dependent thermal expansion coefficient. At higher Reynolds number (and lower Richardson number) the situation reverses, and the effects of temperature-dependent thermal expansion coefficient are larger. Interestingly, there is a range of intermediate situations where the role played by both the viscosity and the thermal expansion coefficient is crucial and of comparable order (see § 4.2).

REFERENCES

ARMENIO, V. & SARKAR, S. 2002 An investigation of stably stratified turbulent channel flow using large-eddy simulation. *J. Fluid Mech.* **459**, 1.

ARYA, S. P. S. 1975 Buoyancy effects in an horizontal flat-plate boundary layer. *J. Fluid Mech.* **68**, 321.

BIAU, D. & BOTTARO, A. 2004 The effect of stable thermal stratification on shear flow stability. *Phys. Fluids* **16**, 4742.

COLEMAN, G. N., FERZIGER, J. H. & SPALART, P. R. 1992 Direct simulation of the stably stratified turbulent Ekman layer. *J. Fluid Mech.* **244**, 677.

FERNANDO, H. J. S 1991 Turbulent mixing in stratified fluids. *Annu. Rev. Fluid Mech.* **23**, 455.

FERZIGER, J. H., KOSEFF, J. R. & MONISMITH, S. G. 2002 Numerical simulation of geophysical turbulence. *Comput. Fluids* **31**, 557.

FRITTS, D. C. & ALEXANDER, M. J. 2003 Gravity wave dynamics and effects in the middle atmosphere. *Rev. Geophys.* **41**, 1003.

GAGE, K. S. & REID, W. H. 1968 The stability of thermally stratified plane Poiseuille flow. *J. Fluid Mech.* **33**, 21.

GARG, R. P., FERZIGER, J. H., MONISMITH, S. G. & KOSEFF, J. R. 2000 Stably stratified turbulent channel flow. I. Stratification regimes and turbulence suppression mechanism. *Phys. Fluids* **12**, 2569.

GERZ, T. & YAMAZAKI, H. 1993 Direct numerical simulation of buoyancy-driven turbulence in stably stratified fluid. *J. Fluid Mech.* **249**, 415.

HERBERT, T. 1983 secondary instability of plane channel flow to subharmonic three-dimensional disturbances. *Phys. Fluids* **26**, 871.

HOLT, S. E., KOSEFF, J. R. & FERZIGER, J. H. 1992 A numerical study of the evolution and structure of homogeneous stably stratified sheared turbulence. *J. Fluid Mech.* **237**, 499.

IIDA, O., KASAGI, N. & NAGANO, Y. 2002 Direct numerical simulation of turbulent channel flow under stable density stratification. *Intl J. Heat Mass Transfer* **45**, 1693.

INCROPERA, F. P. & DEWITT, D. P. 1985 *Fundamentals of Heat and Mass Transfer*. John Wiley and Sons.

KOMORI, S., UEDA, H., OGINO, F. & MIZUSHINA, T. 1983 Turbulence structure in stably stratified open-channel flow. *J. Fluid Mech.* **130**, 13.

LESSANI, B. & ZAINALI, A. 2009 Numerical investigation of stably-stratified turbulent channel flow under non-Boussinesq conditions. *J. Turbul.* **10**, 1.

LIENHARD V, J. H. & VAN ATTA, C. W. 1990 The decay of turbulence in thermally stratified flow. *J. Fluid Mech.* **210**, 57.

METAIS, O. & HERRING, J. R. 1989 Numerical simulations of the freely evolving turbulence in stably stratified fluids. *J. Fluid Mech.* **202**, 117.

POPIEL, C. O. & WOJTKOWIAK, J. 1998 Simple formulas for thermophysical properties of liquid water for heat transfer calculations (from 0 °C to 150 °C). *Heat Transfer Engng* **3** (19), 87.

ROHR, J. J., ITSWEIRE, E. C., HELLAND, K. N. & VAN ATTA, C. N. 1988 Growth and decay of turbulence in a stably stratified shear flow. *J. Fluid Mech.* **195**, 77.

SAIKI, E. M., BIRINGEN, S., DANABASOGLU, G. & STREETT, C. L. 1993 Spatial simulation of secondary instability in plane channel flow: comparison of K- and H-type disturbances. *J. Fluid Mech.* **253**, 485.

SAIKI, E. M., MOENG, C. H. & SULLIVAN, P. P. 2000 Large-eddy simulation of the stably-stratified planetary boundary layer. *Boundary-Layer Meteorol.* **95**, 1.

SOLDATI, A. & BANERJEE, S. 1998 Turbulence modification by large-scale organized electrohydrodynamic flows. *Phys. Fluids* **10**, 1743.

TAYLOR, J. R., SARKAR, S. & ARMENIO, V. 2005 Large eddy simulation of stably stratified open channel flow. *Phys. Fluids* **17**, 116602.

TURNER, J. S. 1973 *Buoyancy Effects in Fluids*. Cambridge University Press.

VAN DEER LEE, E. M. & UMLAUF, L. 2011 Internal wave mixing in the Baltic Sea: near-inertial waves in the absence of tides. *J. Geophys. Res.* **116**, C10016.

YEO, K., KIM, B. G. & LEE, C. 2009 Eulerian and Lagrangian statistics in stably stratified turbulent channel flows. *J. Turbul.* **10**, 1.

ZONTA, F., MARCHIOLI, C. & SOLDATI, A. 2012 Modulation of turbulence in forced convection by temperature-dependent viscosity. *J. Fluid Mech.* **697**, 150–174.